AMERICAN UNIVERSITY OF BEIRUT

DEVELOPING LAND USE REGRESSION MODELS TO PREDICT NITROGEN OXIDES AND OZONE CONCENTRATIONS ACROSS AN URBANIZING GRADIENT: THE CASE OF LEBANON

by
CELINE WAJIH EL KHOURY

A thesis
submitted in partial fulfillment of the requirements
for the degree of Master of Science in Environmental Sciences
to the Interfaculty Graduate Environmental Science Program
(Environmental Technology)
of the Maroun Semaan Faculty of Engineering and Architecture
at the American University of Beirut

Beirut, Lebanon
April 2019

AMERICAN UNIVERSITY OF BEIRUT

DEVELOPING LAND USE REGRESSION MODELS TO PREDICT NITROGEN OXIDES AND OZONE CONCENTRATIONS ACROSS AN URBANIZING GRADIENT: THE CASE OF LEBANON

by

CELINE WAJIH EL KHOURY

Approved by:

Dr. Ibrahim Alameddine, Assistant Professor — Advisor
Department of Civil and Environmental Engineering
American University of Beirut

Dr. Mutasem El Fadel, Professor — Member of Committee
Department of Civil and Environmental Engineering
American University of Beirut

Dr. Marianne Hatzopoulou, Associate Professor — Member of Committee
Department of Civil and Mineral Engineering
University of Toronto

Signing on behalf of Dr. Hatzopoulou.

Date of thesis defense: April 18, 2019

AMERICAN UNIVERSITY OF BEIRUT

THESIS, DISSERTATION, PROJECT RELEASE FORM

Student Name:

El Khoury	Celine	Wajih
Last	First	Middle

☒ Master's Thesis ☐ Master's Project ☐ Doctoral Dissertation

☒ I authorize the American University of Beirut to: (a) reproduce hard or electronic copies of my thesis, dissertation, or project; (b) include such copies in the archives and digital repositories of the University; and (c) make freely available such copies to third parties for research or educational purposes.

☐ I authorize the American University of Beirut, to: (a) reproduce hard or electronic copies of it; (b) include such copies in the archives and digital repositories of the University; and (c) make freely available such copies to third parties for research or educational purposes after:

One ---- year from the date of submission of my thesis, dissertation, or project.
Two ---- years from the date of submission of my thesis, dissertation, or project.
Three ---- years from the date of submission of my thesis, dissertation, or project.

Celine 6 May 2019

Signature Date

ACKNOWLEDGMENTS

I would like to express my gratitude to my advisor, Dr. Ibrahim Alameddine for its guidance and knowledge provided during the completion of this thesis, to Dr. Mutasem El Fadel and Dr. Marianne Hatzopoulo for their positive feedback and constructive comments.

I am also grateful to Ms. Rania Chatila and Mr. Chadi Assaf for their constant help in the CRSL (Central Research Science Laboratory). I would also like to thank to Mr. Ramez Zayyat and Mr. Joseph Daoud for their help and assistance in the environmental engineering laboratory at the Maroun Semaan Faculty of Engineering and Architecture. My recognition and gratitude are also addressed to the URB (University Research Board) for its financial support. I also thank all my friends who have stood by me throughout these past three years. Last but not least, my biggest gratitude goes to my parents, my sisters and my boyfriend who have supported me and kept up with my moodiness and stress during the writing of this thesis.

AN ABSTRACT OF THE THESIS OF

Celine El Khoury for Master of Science in Environmental Sciences
Major: Environmental Technology

Title: Developing land-use regression models to predict nitrogen oxides and ozone concentrations across an urbanizing gradient: the case of Lebanon

Most developing countries suffer from elevated ambient traffic-related air pollution. In the Greater Beirut Area (GBA), the absence of a functioning fixed-station air quality monitoring network with an adequate spatial coverage has curtailed the assessment of personal exposure to air pollutants. The development of Land Use Regression (LUR) models that can predict the intra-urban variability in ambient pollution surfaces as a function of traffic, meteorological and GIS-based explanatory variables have proven effective and efficient. The models have been successfully used and applied across cities in North America, Europe and Asia. In this study, nitrogen oxides (NO_x), nitrogen dioxides (NO_2) and ozone (O_3) concentrations were monitored across the GBA over a year using passive air quality samplers. The annual average concentrations of NO_x and NO_2 in the study area were 89.7 and 36.0 ppb respectively. These concentrations are higher than levels reported across most European and many Asian cities. On the other hand, O_3 concentrations were largely low (GBA wide mean was 26.9 ppb), particularly in the dense and congested urban areas of the GBA. Based on these measurements, annual and seasonal LUR models were developed for the study area. Traffic related predictors were found to have a strong predictive role across all LUR models. Moreover, the role that local point sources had on the ambient levels was also evident in the final model structures. Overall, the performance generated models was good with low biases, a high model robustness, and acceptable R^2 that ranged between 0.66 and 0.73 for NO_2, 0.56 and 0.60 for NO_x, and 0.54 and 0.65 for O_3. The developed LUR models were then used to develop the first ambient pollution concentration maps for the study area for NO_2, NO_x and O_3.

CONTENTS

ILLUSTRATIONS

Figure Page

TABLES

Table Page

CHAPTER 1
THEORETICAL BACKGROUND

1.1 Introduction

The World Health Organization (WHO) estimates that exposure to urban air pollution – or ambient air pollution – was responsible for the death of 4.2 million people per year (WHO, 2018). The WHO also estimates that 91% of the world's population inhales air that exceeds its set health standards (WHO, 2018). As a result, urban air pollution has been linked to the loss of billions of dollars associated with medical costs and loss of productivity (UNEP, 2014). Research conducted by the WHO have shown that nine out of ten people breathe polluted air, which causes the premature death of around 7 million per year. One third of these deaths are caused by strokes, lung cancer and heart diseases (WHO, 2019). Several studies have also shown a direct association between traffic-related air pollution and lung development in children (Bravo, Son, de Freitas, Gouveia, & Bell, 2016; Goldizen, Sly, & Knibbs, 2016).

Combustion reactions contribute significantly to the emissions of different air pollutants. Typical transportation related air pollutants include sulfur dioxide (SO_2), nitrogen oxides (NO and NO_2 as NOx), carbon monoxide (CO), volatile organic compounds (VOCs), and particulate matter (PM). Air pollutants are often divided into primary and secondary pollutants. Primary pollutants are directly emitted into the atmosphere, while secondary pollutants are formed in the atmosphere as a result of chemical reactions with other pollutants. While most of the emitted air pollutant are considered as primary (NO, SO_2, CO, VOCs, PM), ozone (O_3) and nitrogen dioxide (NO_2)

are considered both primary and secondary pollutants (Holman, 1999). It is important to note that nitrogen dioxide and ozone are inter-related, whereby NO_2 is considered the primary source of the oxygen atoms used for ozone formation. Moreover, the formed ozone can easily react with nitric oxide to reproduce nitrogen dioxide and oxygen. As such, there is often a negative correlation between the nitrogen dioxide and ozone concentrations present in the atmosphere (NASA, 2003).

NO_2 is part of a highly reactive group of gases known as nitrogen oxides (NO_x). NO_2 is mainly emitted during combustion reactions that take place in cars, buses, trucks, power plants and any off-road equipment. Prevalent meteorological conditions play an important role in determining the concentration of NO_2 in the atmosphere. High levels of NO_2 are often associated with conditions that are conducive to accumulation and stagnation. As such, NO_2 levels often peak in the winter season due to limited mixing in the lower air boundary and a drop in the photochemical activity (Hargreaves, Leidi, Grubb, Howe, & Mugglestone, 2000). Additionally, higher NO_2 levels tend to occur in the winter due to increased usage of heating and cars. In terms of spatial variability, high concentrations of NO_2 are expected in industrial areas and in the vicinity of major roads and highways (Atari, Luginaah, Xu, & Fung, 2008).

High levels of NO_2 in the ambient air irritate the human respiratory system. In fact, short-term exposure to NO_2 polluted air can worsen respiratory problems, especially asthma (EPA, 2016). On the other hand, long-term exposure to elevated levels of NO_2 can promote the development of asthma and increase proneness to respiratory infections (EPA, 2016). Extended exposure to high levels of PM and NO_2 was also found to induce structural changes in the heart, namely hypertrophy of the left and right ventricle (Cascio, 2016). In

Copenhagen, a 20% reduction in traffic-related NO_2 was found to have increased the life expectancy on average by 0.3 – 0.5 years due to a decrease in ischemic heart diseases, chronic obstructive pulmonary disease (COPD), and asthma (Brønnum-Hansen et al., 2018).

Ozone can be found both at the stratospheric level and at tropospheric level. While the ozone that is naturally present in the stratosphere acts as a protective layer that shields the earth from the dangerous ultraviolet rays, ozone in the troposphere that is formed by chemical reactions between nitrogen oxides and volatile organic compounds (VOCs) is an anthropogenic pollutant. Meteorological parameters directly affect the behavior of O_3. Studies have shown that O_3 tends to stagnate and accumulate in the troposphere when temperatures are high. In fact, high temperatures and sunlight catalyze ozone formation. Ozone accumulation in the atmosphere is also linked to slow-moving high-pressure weather systems. Ozone is known for its oxidation potential. It can irritate the respiratory system and is linked to many respiratory symptoms such as dyspnea, upper airway irritation, chest tightness and coughing (Chen, Kuschner, Gokhale, & Shofer, 2007). Jerrett, Burnett, et al. (2009) showed that increased concentrations of ground-level ozone were significantly related to higher death risks from cardiopulmonary diseases. A systematic review conducted by Zhao, Markevych, Romanos, Nowak, and Heinrich (2018) found inconclusive evidence that associated high levels of ozone with increases in autism spectrum disorders, damage of cognitive functions and dementia, depression and suicide. Nonetheless, chronic health effects of exposure to ozone are not as conclusive as acute ones when it comes to lung function decrements, inflammation, permeability and mild bronchoconstriction. This is mainly due to the confounding effects of different pollutants

present in the atmosphere and the various meteorological parameters (Nuvolone, Petri, & Voller, 2018).

While air pollution monitoring is critical towards assessing exposure and identifying pollution hotspots, there is increased evidence that fixed monitoring network lack the needed spatial coverage to capture the variability of air pollution levels within a city (Kanaroglou et al., 2005). Gulliver and Briggs (2004) have highlighted the potential mismatch between predicted air pollution levels generated from fixed-site monitoring stations and measured levels in the transport microenvironments. Similar conclusions have been reached by K. Miller et al. (2007) who found that the variability of air pollution within cities can often be larger than the variability observed between cities. Given these shortcomings of fixed-monitoring, there has been much work that aimed towards the development of models that can generate accurate pollution surfaces in urban areas. These spatially explicit surfaces can then be used to assess exposure levels and identify key pollution sources. Different types of modeling frameworks have been developed over the years. These include 1) proximity-based assessments, 2) statistical interpolation, 3) land use regression models, and 4) line dispersion models (DM) (Kanaroglou et al., 2005). Proximity-based models are the coarsest as they link air pollution from the nearest monitoring site directly to receptor. On the other hand, interpolation models estimate the concentration surfaces of the target pollutant using geospatial auto-correlations. Land use regression (LUR) models are based on multiple linear regression models that establish relationships between air pollution concentration on one hand and land use, meteorology, transportation, and population on the other (Parenteau, 2012). Dispersion models are mechanistic mathematical tools that predict pollutant concentrations by accounting for

emission, dispersion, and decay (Hassan, 2013). While dispersion models can provide a high spatio-temporal resolution for the predicted air pollutant concentrations, they often tend to be limited by data availability and over-parametrization. In a review that evaluated the four different modeling techniques used for intra-urban air pollution exposure Kanaroglou et al. (2005) showed that LUR models provides consistent estimations of traffic-related air pollution, specifically if enough land-use, transportation and pollution monitoring data were available. The previous methods are not the only ones used in air pollution studies. The latter include the use of spatial interpolation approaches, inverse distance weighting, Kriging, data driven spatial prediction (Xie et al., 2017).

LUR models have been successfully used as an exposure assessment tool to estimate concentration at unmonitored locations in several air pollution monitoring and exposure studies. They have also been used to examine the relationship between observed air pollution concentrations and predictor variables, like land use, meteorology, and traffic parameters. It is important to note that LUR models can make use of data collected at different spatial and temporal scales. The skill of LUR models to predict the spatial variability of NO_2, NO_x and O_3 concentrations in an urban environment is high. The reported R^2 for NO_2 vary between 55% and 92% (Beelen, Hoek, Vienneau, Eeftens, Dimakopoulou, Pedeli, Tsai, Künzli, Schikowski, Marcon, Eriksen, et al., 2013; Kashima, Yorifuji, Sawada, Nakaya, & Eboshida, 2018; Lee et al., 2014; Rahman, Yeganeh, Clifford, Knibbs, & Morawska, 2017; Wolf et al., 2017), between 49 and 92% for NO_x (Beelen, Hoek, Vienneau, Eeftens, Dimakopoulou, Pedeli, Tsai, Künzli, Schikowski, Marcon, Eriksen, et al., 2013; Lee et al., 2014; Rahman et al., 2017), and between 65 and 92% for

O_3 (Berman, Breysse, White, Waugh, & Curriero, 2015; Huang, Zhang, & Bi, 2017; Jerrett, Burnett, et al., 2009; Wolf et al., 2017).

Given the low cost and ability of LUR models to predict the spatial variability of the 3 concerned pollutants, LUR models will be developed for the GBA. Separate multiple linear regression based LUR models are therefore developed for each air pollutant as typically done in the literature (e.g. Beelen, Hoek, Vienneau, Eeftens, Dimakopoulou, Pedeli, Tsai, Künzli, Schikowski, Marcon, & others, 2013; Dirgawati et al., 2016; Gilbert, Goldberg, Beckerman, Brook, & Jerrett, 2005; Sider et al., 2013; Weichenthal et al., 2016). The generated pollution surfaces are also compared to assess the spatial autocorrelation between the thre pollutants. The relative importance of different landuses, weather parameters, and traffic related predictors are then quantified so as to identify the major factors controlling ambient air pollution levels within the study area for each of the three monitored pollutants. The final LUR models are then used to generate continuous surfaces of air pollution levels for the GBA that are used to identify pollution hotspots. The development of these models will help us cover the lack of monitoring coverage, and let us assess the spatio-temporal variability of the concerned pollutants.

CHAPTER 2
METHODOLOGY

2.1 Study Area

The Greater Beirut Area (GBA) is the most populated region in Lebanon, extending over an area of 233 Km^2. It encompasses the capital city of Beirut along with its surrounding suburbs. The GBA extends across an elevation gradient, starting at the coast and reaches up to 800 m above mean sea level. While Beirut and its immediate suburbs are densely populated and highly urbanized, areas further away from the city tend to be less urbanized, especially towards higher elevations. The predominate landuse/lancover across these highland regions tends to be pine forests. Nevertheless, many of these regions are being urbanized at an alarming rate given socio-economic drivers and the lack of an overall master plan to regulate urbanization across the GBA. Note that the Rafic Hariri International Airport (8 km^2) is located within the GBA and it was excluded from the study.

In Lebanon, most urban areas suffer from poor air quality. The Lebanese Ministry of Environment has reported that the transportation sector was responsible for a significant percentage of the national emissions (Ministry of Environment, 2011). Several studies have monitored and analyzed the urban air pollution levels (Table 1); yet the characterization of their spatio-temporal variability remains poorly understood. Farah et al. (2014) collected and analyzed a time series of daily urban air pollutant levels (including NO, NO_2, and O_3) in Beirut. They reported a mean concentration of 30.83 $\mu g/m^3$ for NO, 35.24 $\mu g/m^3$ for NO_2, and 36.34 $\mu g/m^3$ for O_3 (Farah et al., 2014). Badaro-Saliba et al. (2014) reported that the NO_2 levels in Beirut varied between 35 and 67 $\mu g/m^3$, with a mean of 53 $\mu g/m^3$. Abdallah,

Sartelet, and Afif (2016) explored the influence of boundary conditions and anthropogenic emission inventories over the Lebanese territory. They reported a mean hourly ozone concentration of 48.8 μg/m^3 (Abdallah et al., 2016). Additionally, Saliba, Moussa, Salame, and El-Fadel (2006) outlined a monthly average concentrations of ozone, varying between 23 and 34 μg/m^3.

Table 1 Findings of different studies showing the measurements of several pollutants

Pollutant	Range	Mean	Reference
CO (mg/m^3)	2.28 – 63.43	12.57	(Farah et al., 2014)
	1.21 – 2.709	-	(Saliba et al., 2006)
NO (μg/m^3)	0.12 – 391.66	36.34	(Farah et al., 2014)
NO_2(μg/m^3)	0.19 – 137.34	40.37	(Farah et al., 2014)
	35 – 64	53	(Badaro-Saliba et al., 2014)
O_3 (μg/m^3)	2.16 – 74.40	30.83	(Farah et al., 2014)
	-	48.8	(Abdallah et al., 2016)
	23 – 34	-	(Saliba et al., 2006)
PM_{10} (μg/m^3)	4.30 – 334.10	35.24	(Farah et al., 2014)
	44 – 60		(Saliba et al., 2006)
SO_2 (μg/m^3)	0.26 – 70.41	11.11	(Farah et al., 2014)
	13 – 25		(Saliba et al., 2006)
$PM_{2.5}$ (μg/m^3)		20.7	(Abdallah et al., 2016)

Effective monitoring of air quality in the GBA is still poor. The Ministry of Environment launched the Air Quality Monitoring Network in 2013, with the installation of 5 stations. This network will be augmented with the addition of 13 real-time monitoring stations across Lebanon (El Khoury, 2016). While this initiative is a step forward towards assessing air pollution levels in the GBA, it is important to note that maintaining such a monitoring network is expensive and challenging in the Lebanese context.

As such, an air quality sampling campaign was designed to cover 60 pre-defined sites. The selected sites were spatially distributed across the study region to reflect the variability in land use types and road densities within the GBA (Figure 1). Sites were first divided into high, medium and low urban areas based on their landuse/landcover. Sites were then classified in terms of their road densities into high and low road density sites, while ensuring that major roads that have higher traffic counts were given a higher weight as compared to local roads. Selection of the sites in each of the 6 categories was conducted through random stratified sampling using the Spatial Analyst toolbox and the Sampling Tool Design in the ArcGIS 10.6.1 (ESRI 2018). The adopted site selection approach is similar to that conducted in New York City by Matte et al. (2013). The locations of the sampling sites are shown in Figure 1. It should be noted that monitoring at five sites had to be aborted due to security issues and/or recurrent vandalism of equipment.

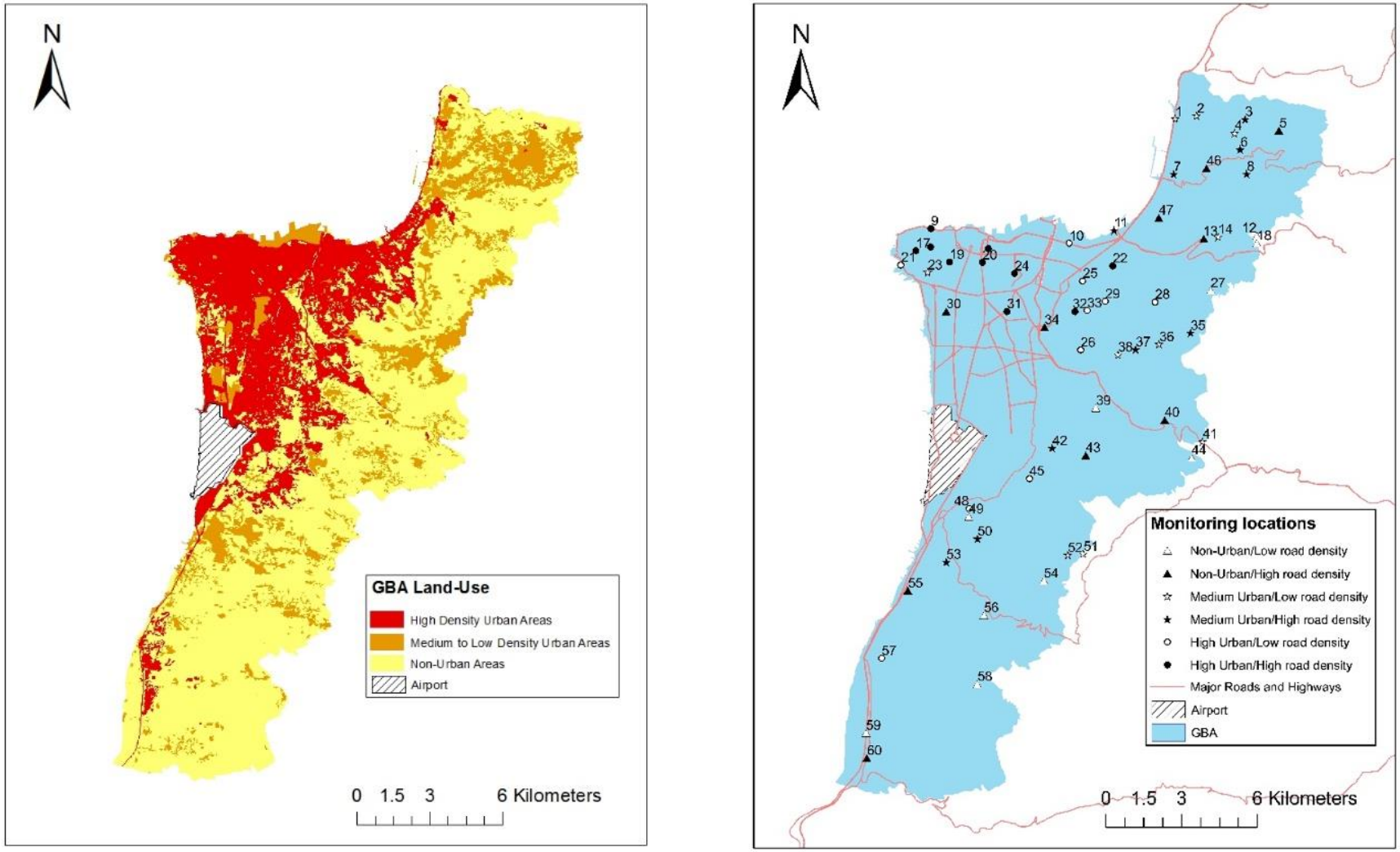

Figure 1. GBA land use for year 2005 (NCRS, 2005)

2.2 Air Quality Sampling Campaign

Ambient concentrations of O_3, NO_2 and NO_x were monitored on a monthly basis starting on August 2017 and ending by July 2018, inclusively. Samples were collected through the use of ambient air passive sampler devices (PSD) manufactured by OGAWA. The passive samplers were chosen as a monitoring tool given their low cost, easy-handling and high precision and accuracy when compared to active methods. OGAWA samplers have been approved by the USEPA after being tested in Houston and El Paso, Texas against the Federal Reference Method (FRM) monitors and photolytic converter (M. E. Sather et al., 2006). A typical OGAWA passive sampler is shown in Figure 2. The OGAWA NO_2 collection filters are made of cellulose fibre, coated with triethanolamine (TEA). While the filters used to measure NO_x are coated with an oxidizing substance: 2-phenyl-4,4,5,5-tetramethylimidazoline-1-oxyl-3-oxide (PTIO) (Annika Hagenbjork-Gustafsson, Andreas Tornevi, Bertil Forsberg, & Kare Eriksson, 2010). The filters used to capture ozone are coated with a nitrite-based solution, thus allowing the oxidizing the nitrite to nitrate. The lowest and highest detectable ranges of the OGAWAs for NO_2, NOx and O_3 are summarized in Table 2.

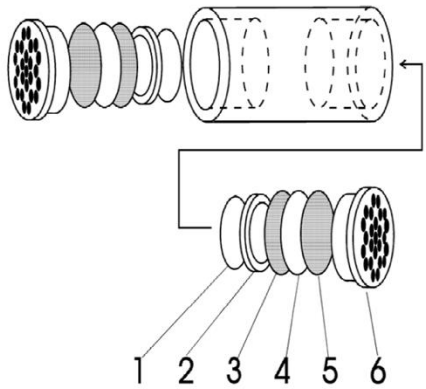

Figure 2. OGAWA ambient passive sampler, 1) solid pad, 2) pad retaining ring, 3) stainless screen, 4) coated collection filet, 5) stainless screen, and 6) diffuser end cap

Table 2. Detectable ranges for concerned pollutants

Pollutant	Lowest detectable range (ppb)		Highest detectable range (ppm)	
NO_2	24 hr 2.3	168 hr 0.32	24 hr 25	168 hr 3.6
NOx	24 hr 2.3	168 hr 0.37	24 hr 5	168 hr 3.6
O_3	24 hr 2.7	168 hr 0.39	24 hr 0.8	168 hr 0.11

OGAWA passive samplers have been tested against other methods of monitoring. When compared with concentrations determined through chemiluminescence instruments, the ratio between the OGAWA concentrations and the chemiluminescence was found to be 1.02 for NO_2 and 1.00 for NOx. In terms of precision, the mean coefficient of variation of NO_2 measurements has been reported to be 6.4% and that of NOx was 3.7% (A. Hagenbjork-Gustafsson, A. Tornevi, B. Forsberg, & K. Eriksson, 2010). When conducting an inter-comparison between the passive samplers and active analyzers, the correlation turned out to be as high as a 0.95 R^2 for NO_2, 0.8 for O_3 and 0.9 for SO_2 (Adon et al., 2010). Given its high performance and accuracy, many studies have based their monitoring

campaigns on the use of passive samplers for measuring NO_2 (Durant et al., 2014; Jerrett, Finkelstein, et al., 2009; Moodley, Singh, & Govender, 2011; Mark E. Sather, Slonecker, Mathew, Daughtrey, & Williams, 2007; Stuart & Zeager, 2011) or O_3 levels (Bytnerowicz et al., 2019; Hagenbjörk, Malmqvist, Mattisson, Sommar, & Modig, 2017; Kerckhoffs et al., 2015; Malmqvist et al., 2014; M. E. Sather et al.; Wolf et al., 2017).

The OGAWA passive samplers were deployed on a monthly basis at each of the 60 defined sampling location. The order by which the identified sites were sampled was randomized for each visit. This aims to reduce biases that may be caused by unaccounted variabilities in traffic and/or weather. The samplers were placed at a height of 1.5 – 2 meter above ground and were placed in an opaque enclosure to protect them from sun, wind, and rain. Moreover, all samplers were located far from local sources of nitrogen oxides like trucks, buses or any combusiton engines and far from walls and other surfaces that might decrease the ozone concentration in the vicinity of the sampler (20 cm from vertical surfaces and 1.5 – 2m above ground) (Ogawa, 2001). The samplers were left in the field for 1 week before collection. Once the PSDs were collected, they were transported and analyzed at the Kamal A. Shair Central Research Science Laboratory at the American University of Beirut. Analysis was done within 14-21 days post collection. The analysis consisted of extracting the NOx, NO_2 and O_3 filters with 8mL of Milli-Q water. The extract of O_3 was analyzed using the Metrohm model 850 professional ion chromatography (IC) with conductivity detector: anion flow of 0.7 mL/min; regenerant pressure 10 psi; nitrogen 99.9% pure at 100 psi; eluant pressure 11 MPa; detector range of 10 µS. The columns used were Metrosep A Supp 7 – 250/4.0 (6.1006.630) with guard column Metrosep RP 2 guard / 3.6 (6.1011.030) and a suppressor MSM rotor (6.2832.000). The retention time of ozone

was at 21±1 minute. The calculation of the time averaged concentration was based on the following equation:

$$O_3(\text{ppm}) = \frac{\text{TN}}{\text{t}} \times \left(\frac{1}{\text{SR}} \times \frac{1\ \mu\text{mol NO}_3}{62\ \mu\text{g NO}_3} \times \frac{1\ \mu\text{mol O}_3}{1\ \mu\text{mol NO}_3} \times \frac{24.45\ \mu\text{L O}_3}{1\ \mu\text{mol O}_3} \times \frac{10^{-6}\text{m}^3\text{O}_3}{1000\ \mu\text{L O}_3} \times \frac{10^6\text{mL O}_3}{\text{m}^3\text{O}_3} \times \frac{10^6\mu\text{L}}{\text{L}}\right)$$

$$= \frac{\text{TN}}{\text{t}} \times 18.09\ \mu\text{L/L}$$

where V is the sample extraction volume in mL, TN is the total nitrate in µg, t is the time in minutes, and SR is the PSD sampling rate for ozone which is equal to 21.8mL/min.

For NO_x and NO_2, the UV-VIS spectrophotometry Agilent 8453 was used for analysis at a wavelength of 540 nm (OGAWA, 2006). In order to calculate time-averaged concentrations of NO_2 and NOx, a standard calibration curve was computed in order to get the slope G. The absorbance of the blank sample was measured (A_b) and then that of the sample (A_b). The actual sample's absorbance is therefore determined as $A = A_s - A_b$. The concentration of the solution is therefore $C_s = A/G$. Once the concentration of the solution is calculated, the collected weight of either NO_2 or NOx can be found in ng, using $m_s = C_s \times V \times 1000$. Finally, the actual time-averaged concentration of either NO_2 or NO_x was calculated using the concentration conversion coefficient (α) that is provided by OGAWA to account for the temperature and relative humidity during the time of field deployment (t) (Equation 1).

$$[NO_2 \text{ or NOx}]\ (\text{ppb}) = \alpha_{NO2\ \text{or}\ NOx} \times m_s \times t \qquad \text{(Equation 1)}$$

Five percent of the PDSs were used as duplicates as part of the QA/QC. Field blanks constituted 10% of the total passive samplers. Both the field blanks and duplicates

were randomly deployed at different sites during each monthly sampling campaign so as to decrease bias (L. Miller et al., 2010).

2.3 Data analysis and LUR model development

Annual-averaged concentrations and seasonally-averaged concentrations were determined. Seasonality was defined in terms of mean monthly ambient temperatures, with measurements taken during the months where average temperatures exceeded 25°C were classified as "hot" season samples, while those below 25°C were categorized as "cold" season samples. The hot season included the months of April, May, June, July and August, while October, November, December, January, February and March constituted the cold season. Statistical differences in the mean and/or median pollution levels between the sites as well as the statistical differences in the variability observed across sites were assessed using the ANOVA and Fligner-Killeen tests respectively. This was also done to assess for the statistical differences between the cold and hot season. In addition, correlation matrices were generated in order to assess the strength of associtaion between the three pollutants. Measured concentrations were also compared to relevant local and international standards (Table 3) to examine the percent exceedances.

Table 3. Ambient Air Quality Standards

Pollutant	**Averaging time**	**MoE NAAQS maximum levels**	**USEPA NAAQS Standards**	**WHO**
Nitrogen dioxide (NO_2)	1 year 24 hours 1 hour	100 µg/m^3 150 µg/m^3 200 µg/m^3	100 µg/m^3 188 µg/m^3	40 µg/m^3 200 µg/m^3
Ground-level Ozone (O_3)	1 hour 8 hours	150 µg/m^3 100 µg/m^3	 75 µg/m^3	 100 µg/m^3

Source: (Ministry of Environment, 2011), (WHO, 2005), (EPA, 2010)

Moran's I was used to assess the global spatial auto-correlation in the collected data and to identify potential spatial clustering in the measured air pollution data. The results were computed using the Moran's I tool in ArcGIS 10.3 (ESRI, 2018a). Moran's I is calculated based on Equation 2 (Ripley, John, & Sons, 2004). Values of Moran's I vary between -1 and 1, whereby values close to -1 indicate clustering of dissimilar values and values close to +1 suggest clustering of similar values. A value of 0 imply randomness or lack of clustering. The statistical significance of the I score was assessed by comparing its z-score against a p-value of 0.05.

$$I = \frac{n \sum_{i=1}^{n} \sum_{j=1}^{n} w_{i,j} z_i z_j}{S_0 \quad \sum_{i=1}^{n} z_i^2} \qquad \text{(Equation 2)}$$

Where z_i is the deviation of an attribute for feature i from its mean; $w_{i,j}$ is the spatial weight between feature i and j, *n* is equal to the number of features, and S_0 is the aggregate of all the spatial weights, as per Equation 3:

$$S_0 = \sum_{i=1}^{n} \sum_{j=1}^{n} w_{i,j} \qquad \text{(Equation 3)}$$

Moreover, Getis-Ord G-statistic was used to identify statistically signficant hotspots and coldspots, given its ability to identify spatial concentrations. The G statistic (z-score) is given by Equation 3 (Getis & Ord, 1992):

$$G_i^* = \frac{\sum_{j=1}^{n} w_{i,j} x_j - \bar{X} \sum_{j=1}^{n} w_{i,j}}{S \sqrt{\frac{[n \sum_{j=1}^{n} w_{i,j}^2 - (\sum_{j=1}^{n} w_{i,j})^2]}{n-1}}} \qquad \text{(Equation 4)}$$

where x_j is the attribute value for feature j; $w_{i,j}$ is the spatial weight between feature i and j; n is equal to the total number of features; $\bar{X} = \frac{\sum_{j=1}^{n} x_j}{n}$, and

$$S = \sqrt{\frac{\sum_{j=1}^{n} x_j^2}{n} - (\bar{X})^2}.$$

The statistical significance of Getis-Ord G was assessed in terms of its z-score. A statistically significant and positive z-score indicated intense clustering of high concentrations in a region that is defined as a hot spot. Statistically significant but negative z-scores suggest intense clustering of low concentration values, which is defined as a potential cold spot.

2.4 LUR model development

Annual and seasonally averaged O_3, NO_2, and NO_x concentrations from the implemented monitoring campaign were used for developing pollutant-specific land-use regression models. The LUR model development followed the methodology outlined in the ESCAPE (European Study of Cohorts for Air Pollution Effects) project, which recommended the use of a supervised stepwise selection procedure (Beelen, Hoek, Vienneau, Eeftens, Dimakopoulou, Pedeli, Tsai, Künzli, Schikowski, Marcon, Eriksen, et al., 2013). As such, each of the pollutant-specific LUR models was fitted using a step-wise multiple linear regression approach, using the “lm” and “step” functions in the R software (RCoreTeam, 2013).

$$Y_{(n)} = X_{(n,k+1)}B_{(k+1)} + \varepsilon_{(n)} \quad \text{(Equation 5)}$$

Where Y represents a vector of n observations; X is a model matrix with k + 1 columns for the predictors, with an initial column of 1 to allow for model intercepts; B is a vector of regression coefficients; and finally e is a vector of model errors (Fox & Weisberg, 2011).

In order to develop the different LUR regression models, potential predictors were chosen based on the findings of previous studies (

Table 4). Predictors were divided into temporally static variables; these included variables such as length of the road within a certain buffer of the sampling site, level of urbanization, forest cover, etc. Several variables were allowed to vary over time such as the predominant meteorological conditions and traffic data. Table 5 summarizes the potential predictors that were considered in the LUR model development. Note that these predictors have been used in previous NO_2, NO_x, and O_3 LUR models and were available in the study area. The buffer distances considered with the collected GIS data were based on the A Distance Decay Regression Selection Strategy (ADDRESS) method proposed by Su, Jerrett, and Beckerman (2009).

Each of the identified predictors was then fitted against the three different pollutants of interest to assess its univariate fit, which was assessed in terms of the generated R^2. The predictor that resulted in the highest R^2 was chosen as the first predictor to enter the model. Others predictors were then added in a forward step-wise fashion, whereby the variable that resulted in the best improvement in the AIC score of the model was chosen. In addition, the sign of the coefficient associated with each predictor was assessed so as to ensure that the relationship had a scientific justification and was not an artifact of overfitting or multicollinearity. Moreover, the addition of any new predictor was assessed in terms of ensuring that it did not change the sign of the slope of any of the previously selected predicts. Predictors that did not follow any of the aforementioned criteria were disregarded. Statistical significance for the inclusion of any predictor was set at the 90% confidence level (p-value ≤ 0.1).

Table 4. Previous LUR models for NOx, NO_2 and O_3

Study area	*Pollutant*	*Model*		*Reference*
		Variables with a positive coefficient	*Variables with a negative coefficient*	
Nanjing, China	NO_2	Residential in 5km buffer	Population in 3km buffer	(Huang et al., 2017)
	O_3	Slope	Longitude	
Japan	NO_2	No. of heavy traffic road in 100 m No. of trucks and large trucks (%) in 200m Average of buses route rate Other in 50m Number of population in 1km	Farmland area in 1km Water in 50m Average slope in 1km	(Kashima et al., 2018)
Brisbane, Austria	NO_2	Population Density Major road Industrial area Distance to major road	Open area Residential area	(Rahman et al., 2017)
	NOx	Open area Industrial area Residential area Distance to major road		
Auckland, NZ	NO_2	No. bus stops in 100m buffer Awnings Street Width	Distance to major road	(Weissert, Salmond, Miskell, Alavi-Shoshtari, & Williams, 2018)
Shangai, China	NO_2	Major road in a 2 km Count of industrial sources in 10 km buffer Population counts	Agricultural land area in 5km	(Meng et al., 2015)

Study area	*Pollutant*	*Model*		*Reference*
		Variables with a positive coefficient	*Variables with a negative coefficient*	
Western Europe	NO_2	Major road in 100 m All roads in 100 m Ports in 800 m Residential in 200m	Natural land in 50 m	(de Hoogh et al., 2018)
	O_3– annual	Major road in 200m Altitude North South trend	Ports in 4 km Residential area in 500m Residential area in 2 km East West trend	
Netherlands	O_3 – annual & summer	North Urban green space 500m buffer	Traffic intensity in 50m buffer Low density residential land in 5km buffer Major road length 50m buffer	(Kerckhoffs et al., 2015)
Augsburg, Germany	O_3	Square root of elevation Number of buildings in 500m	Traffic load in 100m X coordinate Area of buildings Population in 300m	(Wolf et al., 2017)
Montreal, Canada	O_3	Temperature squared Building area 300m Distance to shore Number of bus stops in 100m Length of highway in 100m NOx emissions in 750m	Temperature Distance to port Commercial area in 750m Distance to highway Park area in 1km buffer Wind Speed Distance to major road	(Deville Cavellin et al., 2016)

Table 5. Predictors used for the traffic-related air pollution LURs

Predictor Category	*Predictors*	*Buffer distances in meters*	*Source*
Traffic	Distance to nearest highway	-	NCSR (2005)
	Distance to nearest major road	-	
	Total length of roads	50, 100, 200, 300, 500, 700, 1000, 1500, 2000, 3000	
	Total length of major roads	50, 100, 200, 300, 500, 700, 1000, 1500, 2000, 3000	
	Total length of highways	50, 100, 200, 300, 500, 700, 1000, 1500, 2000, 3000	
Land Use	Percent coverage by residential area (low, medium and high)	50, 100, 200, 300, 500, 700, 1000, 1500, 2000, 3000	NCSR (2005)
	Percent coverage by industrial area	50, 100, 200, 300, 500, 700, 1000, 1500, 2000, 3000	
	Percent coverage by agricultural area	50, 100, 200, 300, 500, 700, 1000, 1500, 2000, 3000	
	Percent coverage by forest area	50, 100, 200, 300, 500, 700, 1000, 1500, 2000, 3000	
	Percent coverage by open spaces	50, 100, 200, 300, 500, 700, 1000, 1500, 2000, 3000	
	Percent coverage by water bodies	50, 100, 200, 300, 500, 700, 1000, 1500, 2000, 3000	
	Percent coverage by high, medium and low urban areas	50, 100, 200, 300, 500, 700, 1000, 1500, 2000, 3000	
	Distance to sea	-	
	Building Density	50, 100, 200, 300, 500, 700, 1000, 1500, 2000, 3000	
Meteorology	Weekly Temperature	-	Rafic Hariri International Airport
	Weekly average wind speed	-	
	Weekly average wind direction	-	
	Weekly relative humidity	-	
Other	Distance to airport	-	NCSR (2005)
	Distance to power plants	-	
	Distance to sea	-	
	Elevation	-	

The generated LUR models were checked against issues of multicollinearity using the variance inflation factor (VIF). Models were deemed appropriate, if their VIF did not exceed 3. Heteroscedasticity, non-normality and influential observations (Cook's D) were assessed for all generated models. The performance of the generated LUR models was assessed in terms of their R^2, adjusted R^2 and the root mean squared errors (RMSE). Additionally, a 4-fold (k-fold) cross-validation assessment was conducted using the "DAAG" package (Maindonald & Braun, 2015) in R to assess the robustness of the final models. The k-fold cross-validation assesses the performance of the model on different subsets of the data and then computes an average of the prediction error rate. The lower the prediction error rate the better the model is. Moreover, the residuals' spatial autocorrelation was evaluated using Moran's I. Finally, the percent bias (PBIAS) for each model was computed and used to check the tendency of the models' to over or under-predict. The final models for each of the three pollutants were then used to generate pollution surfaces for the entire GBA using the R-ArcGIS bridge in ArcGIS and the "arcgisbinding" R package (ESRI, 2018b). All surfaces had a spatial resolution of 100 x 100 m.

CHAPTER 3
RESULTS

3.1 Field measurements

3.1.1 Nitrogen dioxide

Measured NO_2 concentrations in the study area were found to statistically differ across the sampling sites (ANOVA, p-value < 0.05) (Figure 3). Measured concentrations varied between 14.7 ppb at Site 13 and 67.9 ppb at Site 28. Site 13 is located in a low density urban area and is close to the Metn Express Highway (Table 6). On the other hand, Site 28 is located on a secondary road in an area with a high urban density. The temporal variability in NO_2 levels between sites was also significant; Site 2 had the highest variability (standard deviation = 11.16 ppb), while Site 51 showed the lowest variability across time (standard deviation = 2.84 ppb). Seasonally averaged concentrations were found to be largely similar, with no major differences between the cold and hot season levels across sites (Figure 4). The results of the Wilcoxon paired test showed that there was no statistical difference in the median concentrations between the two seasons (p-value > 0.05). Annually averaged NO_2 concentrations were found to range between 22.9 (Site 55) and 53.0 ppb (Site 28). With these concentrations, it is apparent that all monitored sites in the GBA were below the USEPA and the MoE annual standards set for NO_2 (53 ppb). Nevertheless, all sites exceeded the WHO set annual target of 21.3 ppb. The Getis-Ord Gi hot-spot analysis conducted on the annually averaged concentrations, showed that Sites 55 (p-value < 0.01) and 52 (p-value < 0.01) represented statistically significant cold spots, while Sites 10 and 28 were found to be significant hotspot areas (p-value < 0.05) (Figure 5). Seasonally, the hot spot analysis for the

cold season matched the results for the annual analysis, while the results for the hot season differed. In the hot season, Sites 45, 51, 52 and 57 were identified as statistically significant cold spots, while sites 28 and 40 were identified as statistically significant hotspots.

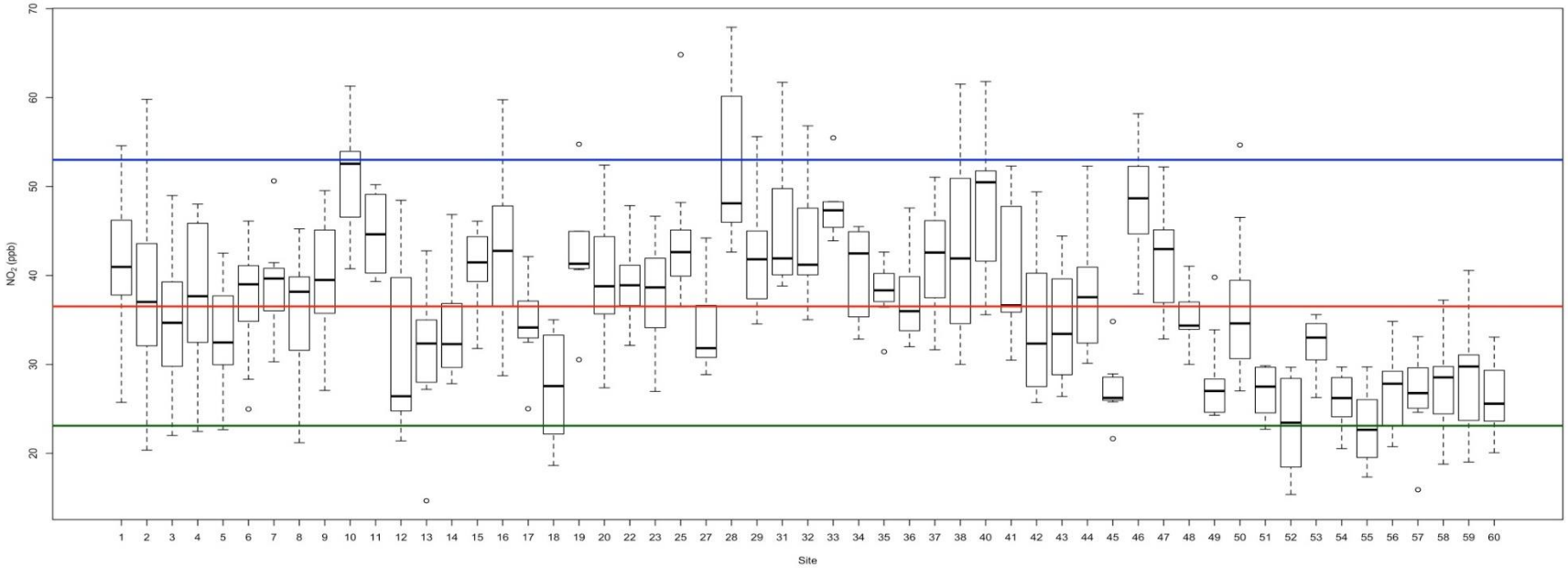

Figure 3. NO_2 variation by site. The blue line represents the USEPA and MoE's annual set standard for NO_2, the green line represents the WHO annual standard, the red line shows the median concentration across all sites.

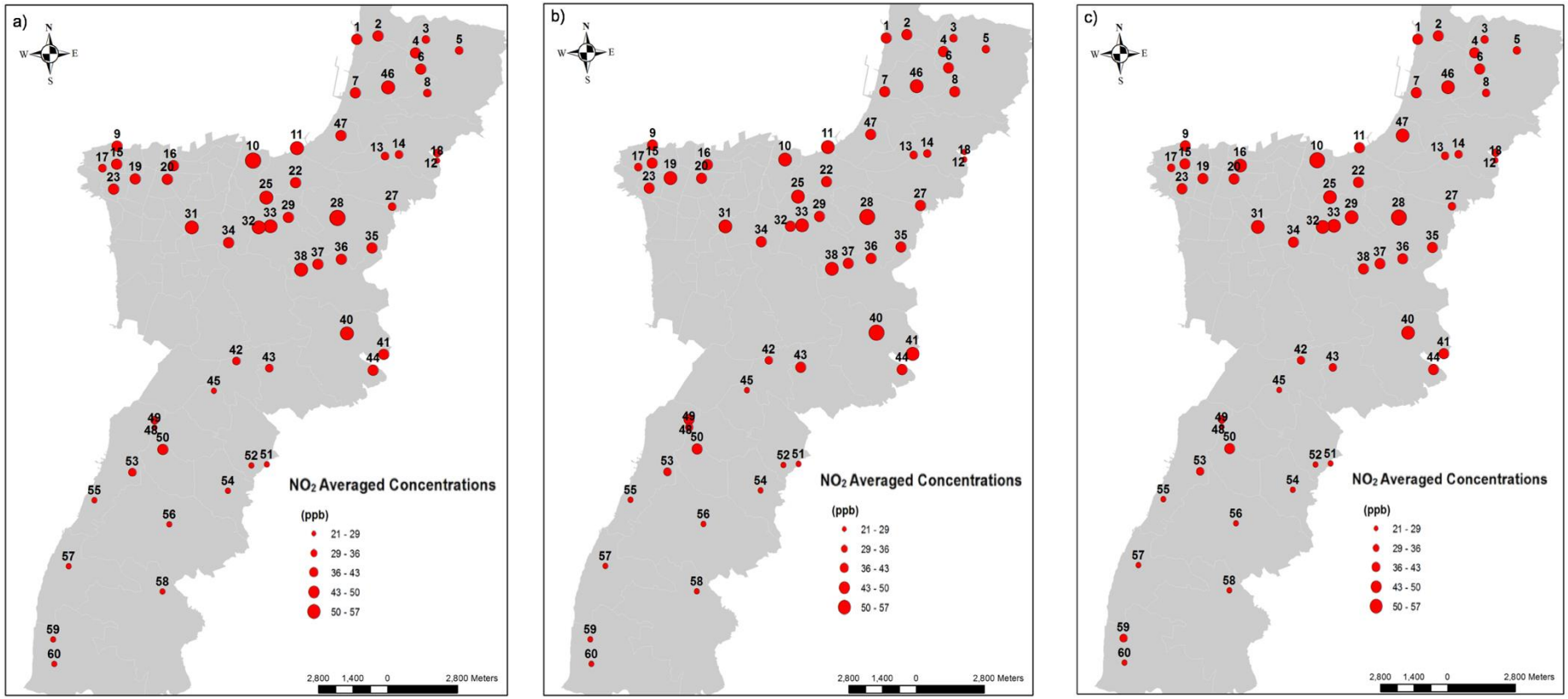

Figure 4. Spatial distribution of NO_2 concentration a) annual-averaged levels, b) hot-season averaged levels, and c) cold-season averaged levels

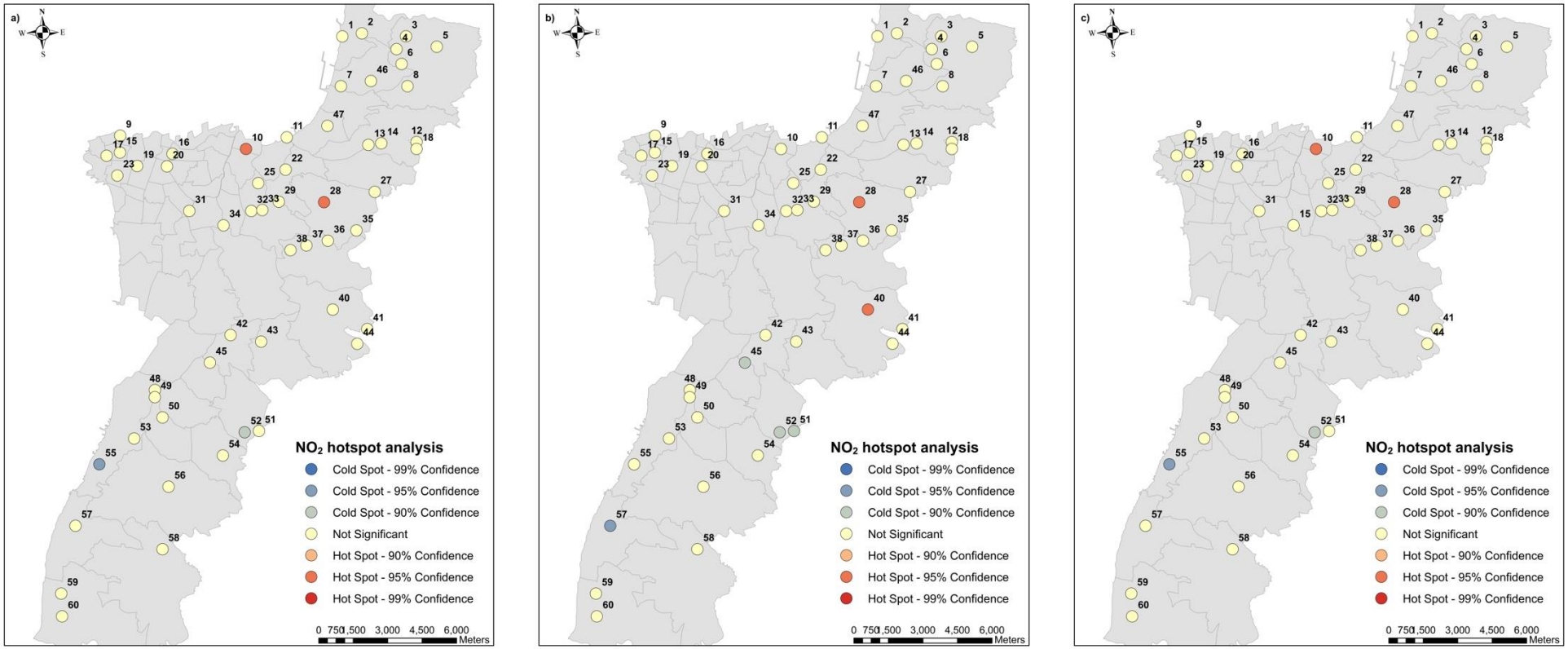

Figure 5. NO_2 cold and hotspots a) annual, b) hot season, c) cold season based on the Getis-Ord Gi* hotspot analysis. Cold-spots (low concentrations) are shown in shades of blue and the hot-spots (high concentrations) in shades of red

3.1.2 Nitrogen oxides

Measured NOx concentrations were found to statistically differ across the sampling sites (ANOVA, p-value < 0.05) (Figure 6). The measured concentrations varied between 25.59 and 270.02 ppb. The lowest recorded NO_x concentration was measured at Site 51, which is located in a medium density urban density with a low road density, while the highest concentration was observed at Site 46, which is located in a low density urban area but with a high road density, most of which are major roads with high traffic volumes. The variability in the measured NO_x levels at each site was not similar; Site 41 had the highest variability (sd =49.4 ppb), while Site 11 showed the lowest variability across time. Similar to NO2, the seasonally averaged concentrations at each sampling site (Figure 7) were not statistically different from each other in the cold and hot seasons (Wilcoxon paired test, p-value > 0.05). Averaged hot season concentrations ranged between 34.9 (Site 54) to 216.21 ppb (Site 40), while cold averaged concentrations ranged between 30.69 (Site 51) and 195.54 ppb (Site 46). Meanwhile, averaged annual concentrations varied between 33.36 for Site 51 and 166.13 ppb for Site 46 (Table 6). Similar to the patterns observed with NO_2, the high NO_x concentrations tended to be positively correlated with road density and traffic, while low concentrations tended to be collocated in regions with both low urban densities and low road density. In fact, the NO_2 and NO_x concentrations were found to be highly correlated. Based on the annually-averaged measurements by site, they had a correlation factor of 0.7 (Table 7). For the cold season, the correlation was slightly lower (0.67), while it was stronger during the hot season with a value of 0.8. The Getis-Ord Gi hot-spot analysis revealed that Sites 10, 40, 41, and 46 were flagged as hotspot regions based on the annually averaged seasonal concentrations (Figure 8). Sites 10, 40 and 41

were identified as hotspots at the 95% confidence interval (p-value < 0.05), while Site 46 was significant at the 99% confidence interval (p-value < 0.01). During the cold and hot seasons, Sites 40 and 41 were found to be hotspots at the 99% confidence interval (p-value < 0.01), while Site 46 was significant at the 95% confidence interval (p-value < 0.05). Site 31 was also found to be a statistically significant hotspot in both seasons (p-value < 0.1). Unlike NO_2, no statistically significant cold spots were identified.

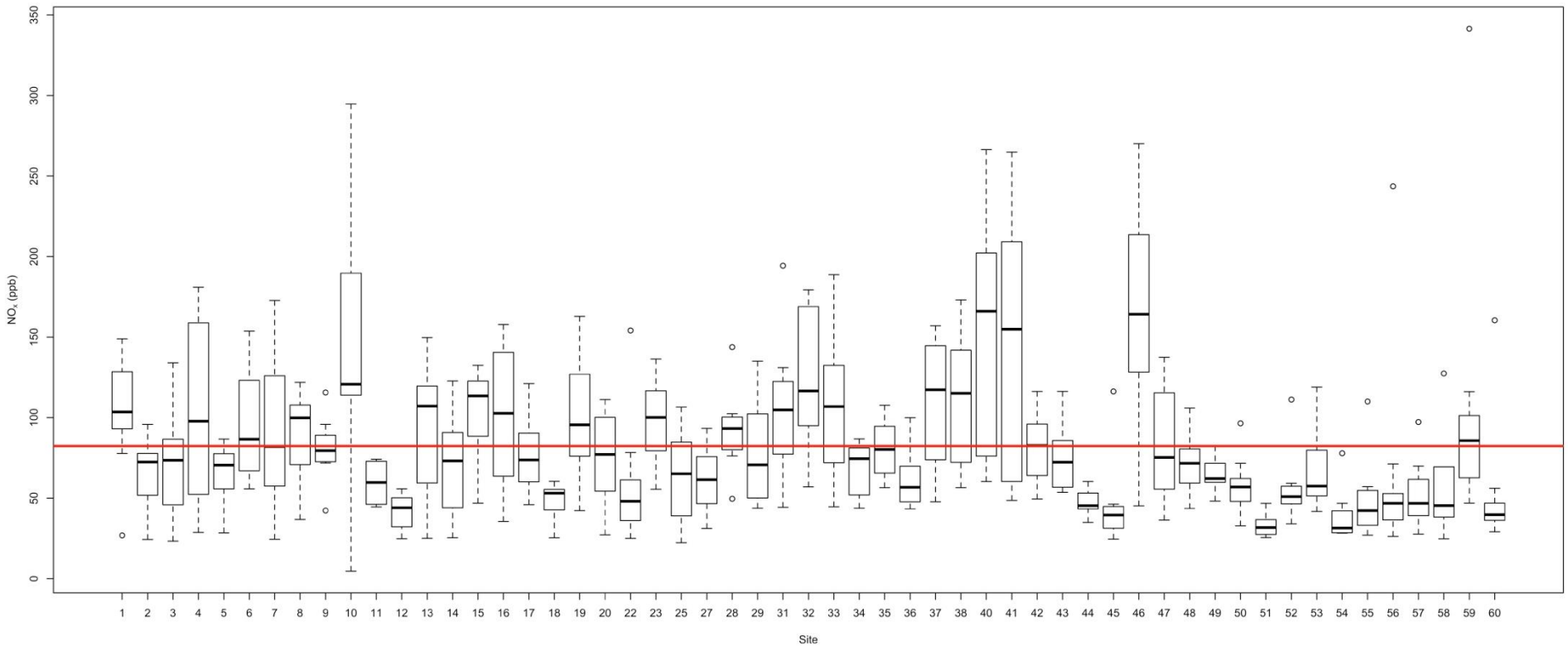

Figure 6. NO_x variation by sampling sites. The red line shows the median concentration across the entire sampling campaign.

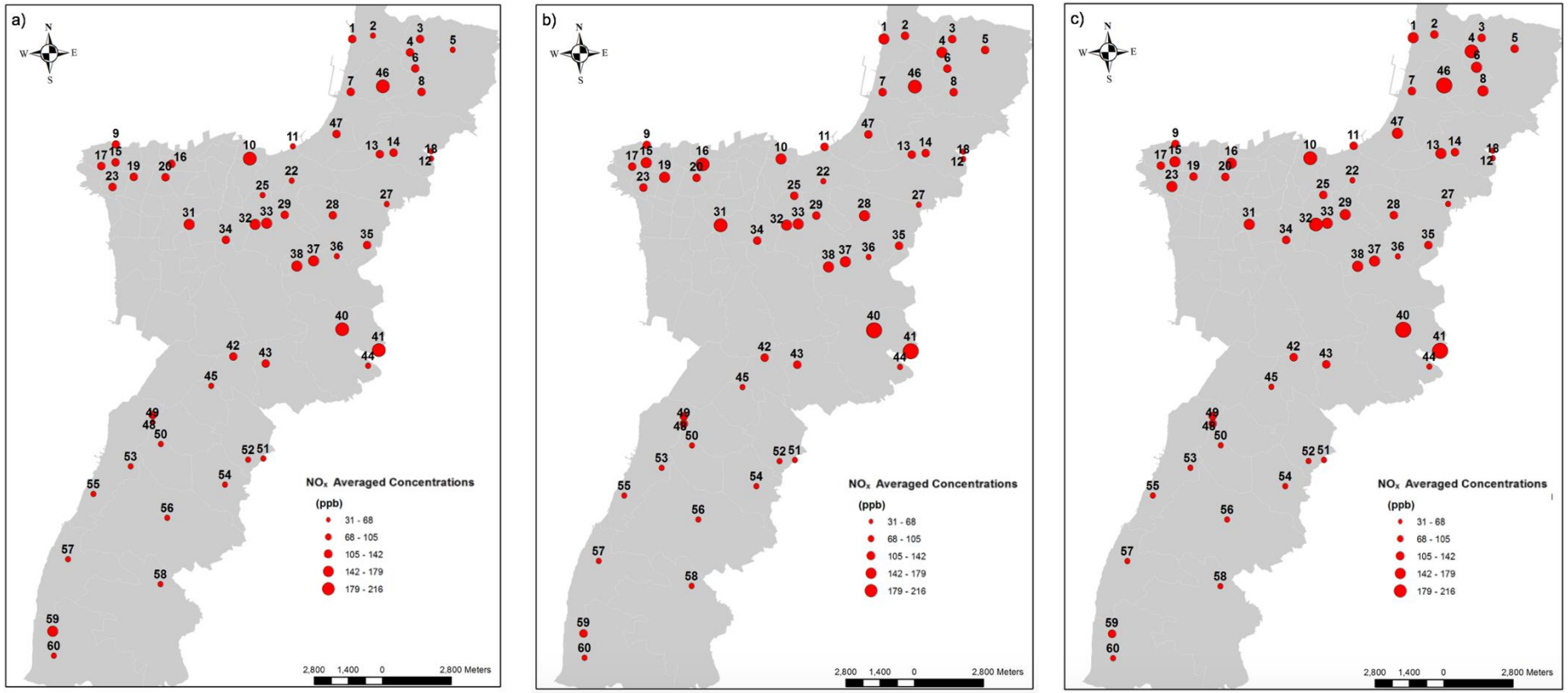

Figure 7. Spatial distribution of NO_x concentration a) annual-averaged levels, b) hot-season averaged levels, and c) cold-season averaged levels

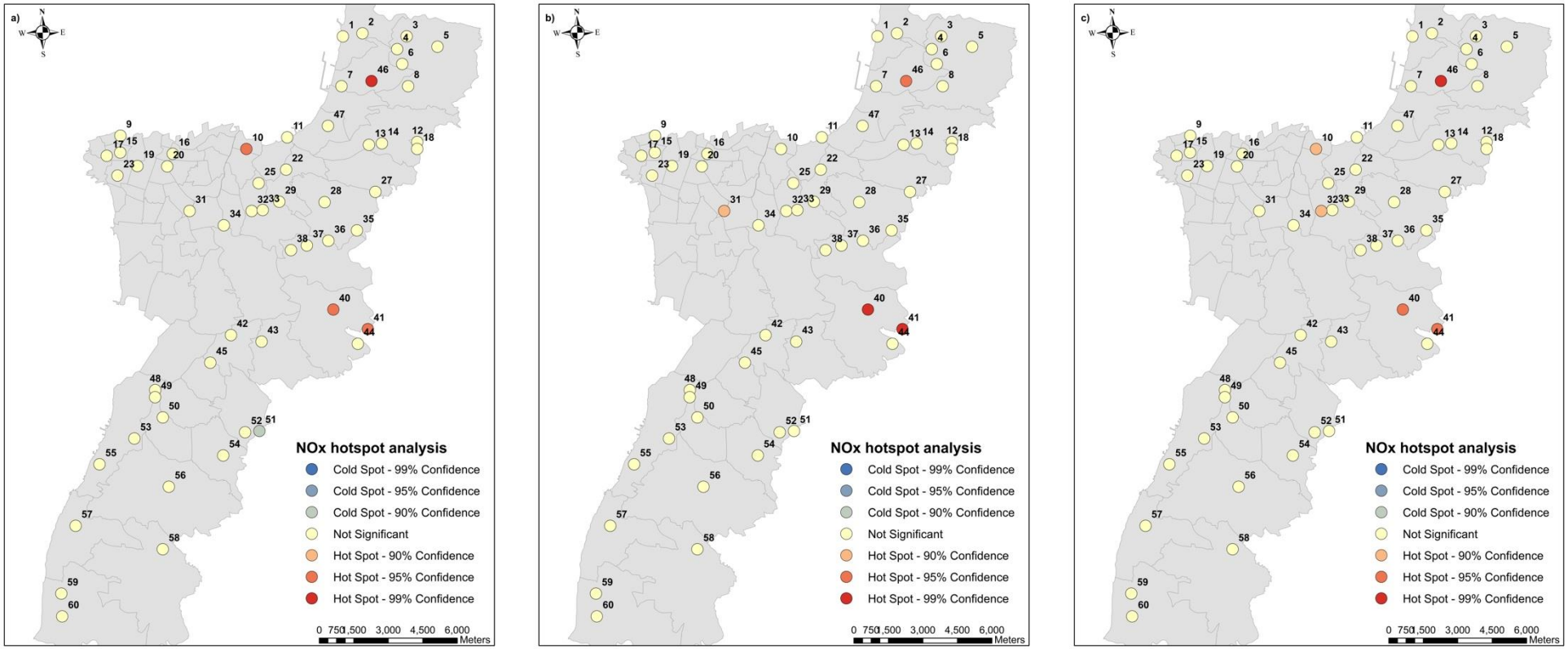

Figure 8. NO_x cold and hotspots a) annual, b) hot season, c) cold season based on the Getis-Ord Gi* hotspot analysis. Cold-spots (low concentrations) are shown in shades of blue and the hot-spots (high concentrations) are shown in shades of red

3.1.3 Ozone

Measured ground-level O_3 concentrations varied significantly between sites (p-value < 0.05); levels ranged between 15.8 and 49.1 ppb at Sites 10 and 51, respectively (Figure 9). The variability of O_3 at each site was also found to be large and statistically varied from site to site. Site 43 was associated with the highest variability (sd =8.56 ppb), while Site 28 recorded the lowest variability across time with a standard deviation of 1.88 ppb. Similar to the NO_2 and NO_x levels, the seasonally averaged O_3 concentrations at each site were not found to be statistically different (Wilcoxon paired test, p-value > 0.05). Site averaged O_3 concentrations in the hot season ranged between 34.9 (Site 54) and 216.21 ppb (Site 40), while cold season averaged concentrations ranged between 30.69 (Site 51) and 195.54 ppb (Site 46) (Figure 10). The annual-averaged concentrations of O_3 ranged between 22.03 (Site 37) and 38.95 ppb (Site 51) (Table 6). Unlike NO_2 and NO_x, the highest concentrations of O_3 were located in low density urban areas with low road densities, while the lowest concentrations were at sites with high urban and road densities with a predominance of major roads. This indicates that the O_3 scavenging pathways dominate over the ground-level O_3 generation pathways. As a matter of fact, O_3 levels were found to be negatively correlated with both NO_2 and NO_x. The correlation coefficient between NO_2 and O_3 was -0.7 for both the annual averaged and cold season concentrations, while the hot season correlation was significantly weaker (-0.21). The same trend was observed between O_3 and NO_x (Table 7).

Measured ground-level ozone concentrations were all below the ambient USEPA (70 ppb), WHO (51 ppb) and MoE (76 ppb) eight-hour standards. The Getis-Ord Gi hotspot analysis conducted on the annually-averaged O_3 concentrations identified that three

sites were statistically identified as hotspots (confidence level > 95%); these sites were Site 51, Site 57 and Site 58. No statistically significant cold spots were identified. A similar pattern was observed for the cold season; yet one statistically significant cold spot was identified, namely Site 32 (90% confidence interval). The site is located in a highly dense urban area with a high road density, most of which are congested. The hot-spot analysis for the hot season showed a larger number of statistically significant cold spots as compared to the identified hot spots (Figure 11). Site 9 was categorized as a hotspot with a 95% confidence interval, while sites 40, 43 and 45 were classified as cold spots with a 95% confidence interval and site 49 with a 90% confidence interval (Figure 11).

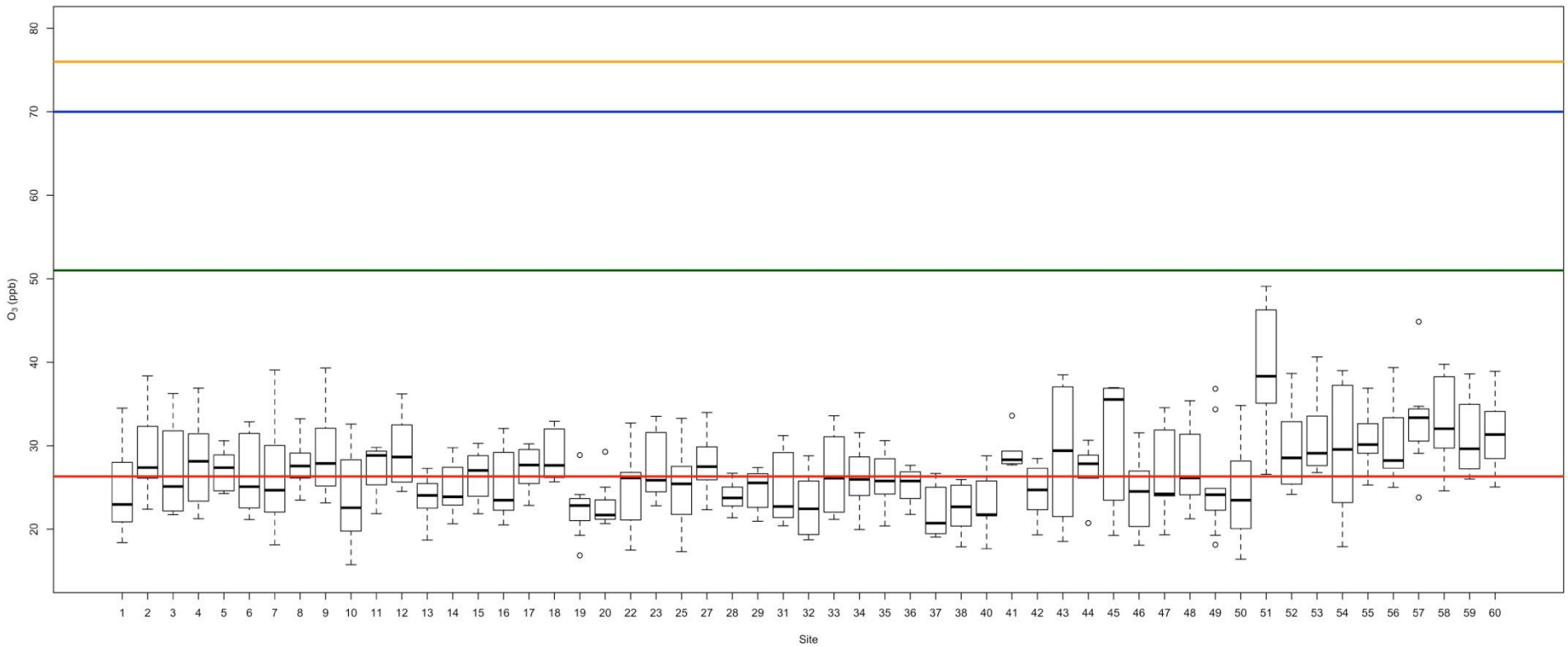

Figure 9. O_3 variation by Site. The red line shows the median concentration of the entire sampling campaign, the green line is the 8-hr WHO standard, the blue line is the USEPA standard and the yellow line is the MoE set standard

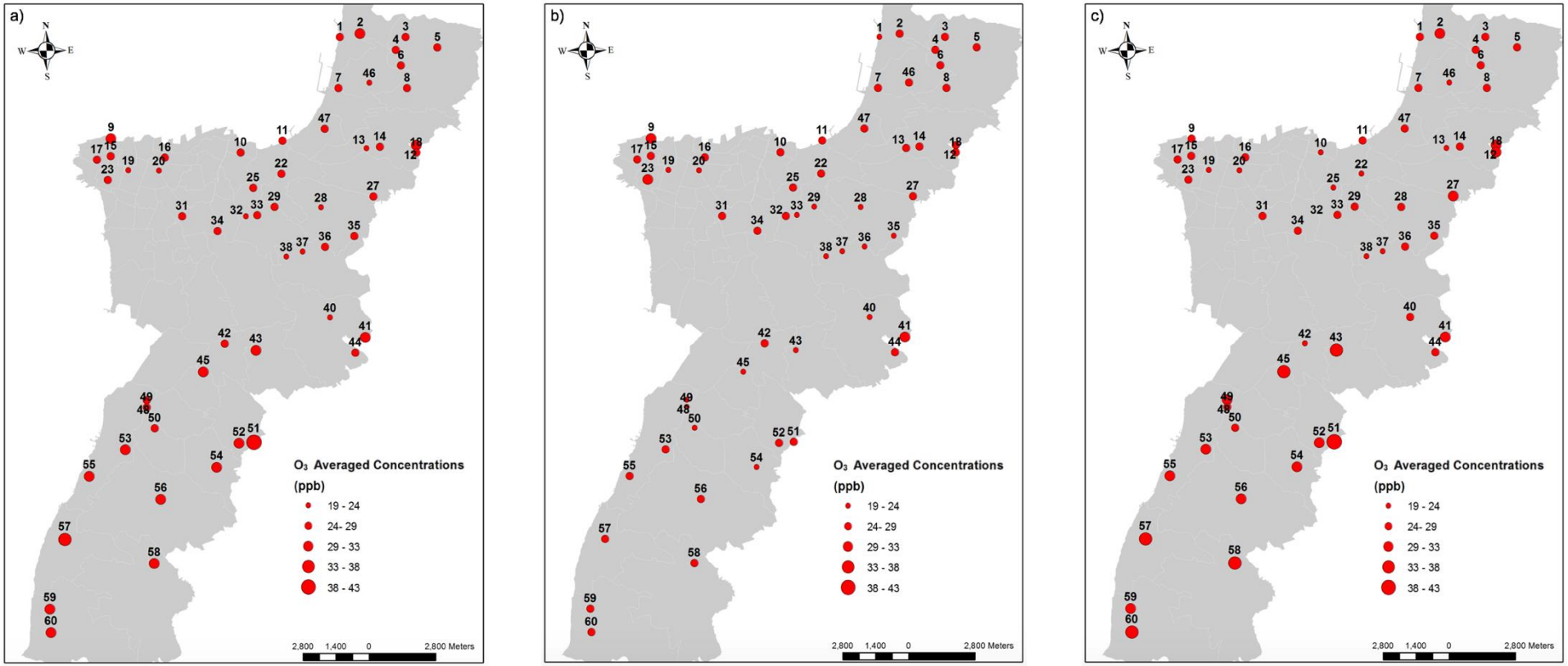

Figure 10. Spatial Distribution of O_3 concentration a) annual-averaged levels, b) hot-season averaged levels, and c) cold-season averaged levels

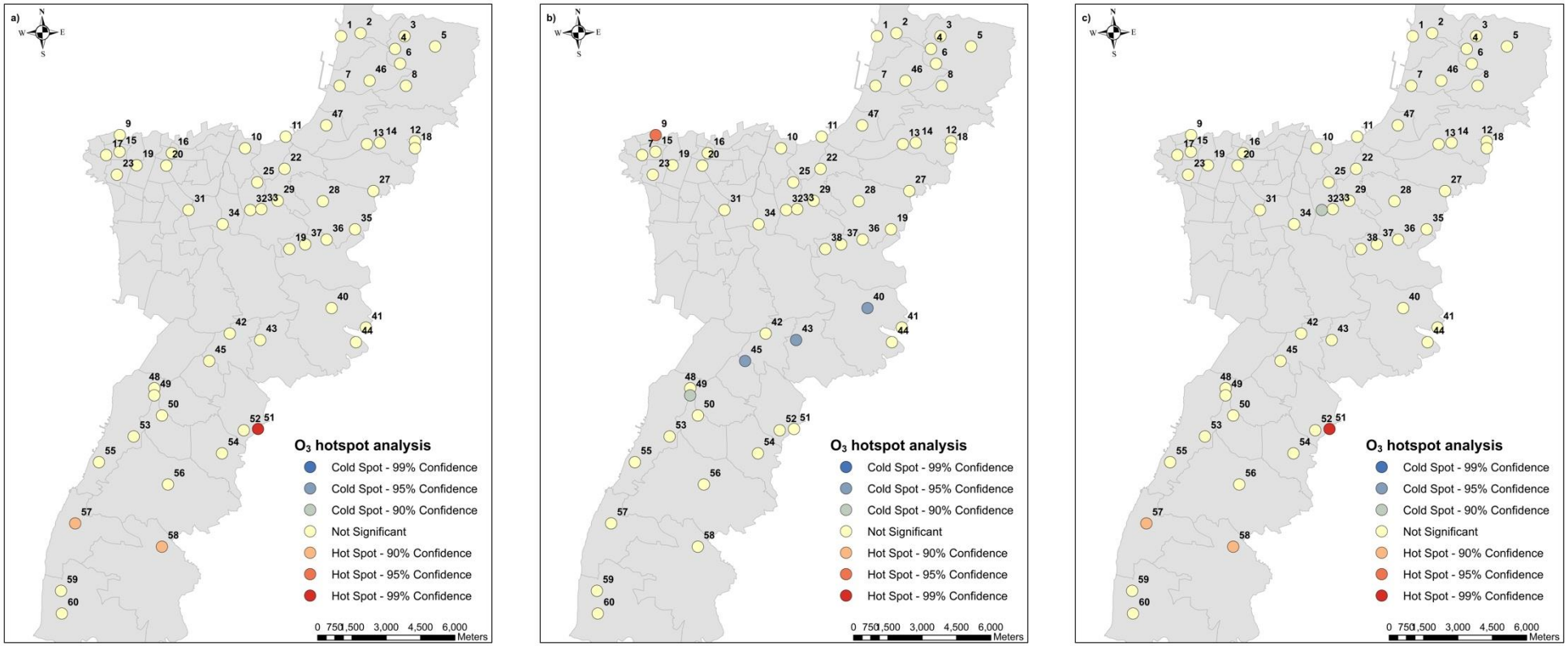

Figure 11. O_3 cold and hotspots a) annual, b) hot season, c) cold season based on the Getis-Ord Gi* hotspot analysis. Cold-spots (low concentrations) are shown in shades of blue, while hot-spots (high concentrations) are presented in shades of red.

Table 6. Summary statistics of the monitored air pollutants

		Minimum (ppb)	Maximum (ppb)	Average (ppb)	Median (ppb)	Standard Deviation (ppb)
Observed	NO_2	14.67	67.91	36.87	36.53	9.44
	NOx	25.59	270.02	89.70	82.36	41.49
	O_3	15.76	49.10	26.90	26.33	5.28
Annual	NO_2	22.87	52.99	36.89	37.63	7.20
	NOx	33.36	166.13	81.30	74.98	29.42
	O_3	22.03	38.95	27.04	26.90	3.20
Cold	NO_2	21.99	54.52	36.75	36.73	7.18
	NOx	30.69	195.54	89.23	78.77	40.02
	O_3	20.47	41.42	27.77	27.31	4.26
Hot	NO_2	21.34	56.14	37.05	38.11	8.06
	NOx	34.90	216.21	90.50	82.23	40.86
	O_3	22.03	38.95	27.04	26.90	3.20

Table 7. Correlation matrix for the three monitored pollutants

		NO_2	NOx	O_3
Annual	NO_2	1.00	0.70***	-0.70***
	NOx	0.70***	1.00	-0.52***
	O_3	-0.70***	-0.52***	1.00
Cold	NO_2	1.00	0.67***	-0.70***
	NOx	0.67***	1.00	-0.60***
	O_3	-0.70***	-0.60***	1.00
Hot	NO_2	1.00	0.80***	-0.21***
	NOx	0.80***	1.00	-0.11***
	O_3	-0.21***	-0.11***	1.00

*** p-value < 0.05

3.2 Land-use regression models

3.2.1 NO_2 land-use regression models

The LUR models developed to estimate the annual averaged NO_2 concentrations as well as the seasonal concentrations are summarized in Table 8. The seasonal and annual models were found to share two predictors namely, the distance to the Zouk power plant and the percent coverage of low urban area within a 300 meter buffer from a site. Both of which were found to be negatively associated with the measured NO_2 concentrations. All three models also included a traffic-related predictor that was found to positively contribute to the NO_2 concentrations. In addition, all three models had prevalent meteorological predictors that helped modulate the NO_2 levels.

Table 8. LUR models of NO_2

	Predictors	Coefficients	t-value	p-value	R^2; Adjusted R^2	RMSE
Annual model: log(NO_2)	(Intercept) Building_3000 (%) Distance_Zouk (km) LUrban_300 (%) Relative_Humidity (%) Major_50 (km)	4.267 4.299×10^{-3} -9.313×10^{-3} -1.553×10^{-2} -1.161×10^{-2} 4.458×10^{-1}	11.85 2.887 -3.443 -2.669 -2.147 2.179	5.33×10^{-16} 0.00578 0.00119 0.01028 0.03678 0.03420	0.68; 0.65	0.11
Hot season model: log(NO_2 hot)	(Intercept) Building_3000 (%) Distance_Zouk (km) Relative_Humidity (%) Lurban_300 (%) Distance_Major (km) Open_3000 (%)	5.099 3.312×10^{-3} -8.340×10^{-3} -2.087×10^{-2} -1.676×10^{-2} -1.612×10^{-1} -1.294×10^{-2}	12.179 1.943 -1.968 -3.522 -2.378 -1.860 -1.794	2.73×10^{-16} 0.057934 0.054834 0.000952 0.021418 0.069028 0.079136	0.66; 0.62	0.13
Cold season model: log(NO_2 cold)	(Intercept) Distance_Zouk (km) Temperature (°C) LUrban_300 (%) Highway_50 (km) Wind_Speed (kph)	2.849 -1.221×10^{-2} 5.141×10^{-2} -1.482×10^{-2} 6.524×10^{-1} -8.385×10^{-3}	17.383 -5.668 5.943 -2.762 2.992 -3.590	$< 2 \times 10^{-16}$ 7.55×10^{-7} 2.87×10^{-7} 0.008063 0.004326 0.000776	0.73; 0.70	0.10

LUrban_300: Percent low urban areas in 300 meters buffer
Distance_Major: Distance to major roads in Km
Major_50: Total length of major roads within a 50 meter buffer (Km)
Building_3000: Percent of area within a 3000 m buffer that is covered by buildings
Open_3000: Percent of area within a 3000 m buffer that is occupied by open areas
Highway_50: Total length of highways within a 50 m buffer (Km)
Distance_Zouk: Distance to the Zouk power plant (Km)

3.2.1.1 NO_2 annual model

The annual NO_2 LUR model incorporated both the effects of the point sources as well as the traffic related emissions in the GBA. The distance to the Zouk power plant, the largest point source emitter in the study areas, was found to correlate negatively with the annual concentrations. This highlight the role that the power plant plays in increasing the NO_2 levels in its immediate surroundings. On the other hand, the percent area occupied by buildings within a 3 km buffer and the length of major roads within a 50-m buffer from a site were found to be positively correlated with NO_2 levels. Both predictors are surrogates of increased urbanization and traffic. The total length of major roads within a 50-m buffer appears to play the dominant role in terms of increasing ambient concentrations; in fact, for every 0.5 Km increase in the length of major roads, the annually averaged NO_2 levels was expected to increase by around 25%. On the other hand, for every 10% increase in the building area coverage within a 3 Km buffer the median NO_2 levels were expected to increase by 4%. As expected, areas experiencing higher relative humidity levels tended to have lower NO_2 concentrations as compared to similar sites with lower humidity levels. Previous work has shown that higher relative humidity levels increase the deposition velocity of NO_2, which results in the increased removal of NO_2 from the atmosphere (Valuntaitė, Šerevičienė, Girgždienė, & Paliulis, 2012). Sites with a higher percentage of low urban density developments within their 300 meter buffer were predicted to have lower NO_2 levels on average as compared to similar sites that are more densely urbanized. A decrease of 10% in low density urban coverage resulted on average in a 17% increase in NO_2 levels. Assessing the LUR-based map clearly shows that that the highest NO_2 concentrations can be found in the immediate vicinity of major roads as seen in Region A

in Figure 12. Concentrations tend to decrease moving away from these roads. Moreover, the region around the Zouk power plant (Region C) also shows medium to high concentrations, even though the distribution of major roads in that part of the GBA is relatively low. As can be seen, the highest concentrations appear to be located within the geographic boundaries of Beirut city, which is the highest urbanized area within the GBA. The lowest concentrations appear to occur in the southern part of the GBA (Region B in Figure 12) and the few remaining villages in the GBA that are associated with low urban densities; the latter appear as blue cold spots in the prediction map. Overall, the model was able to explain 68% of the variability observed in the annually averaged NO_2 concentrations ($R^2 = 0.68$) (Figure 13). The model showed a minor tendency to over-predict pollution levels, with a PBIAS of 4%. The root mean square error of the model was also low (0.1). Finally, in terms of the spatial auto-correlation of the model residuals, the Moran's I index was found to be -0.031 with a z-score of -0.55. This indicated the absence of any clustering and/or spatial auto-correlation in the model residuals. The robustness of the model was assessed through a 4-fold cross-validation; the overall mean squared of the prediction errors (MSPE) was found to be 0.0421, indicating that the model structure was robust in its ability to predict the annual averaged NO_2 concentrations.

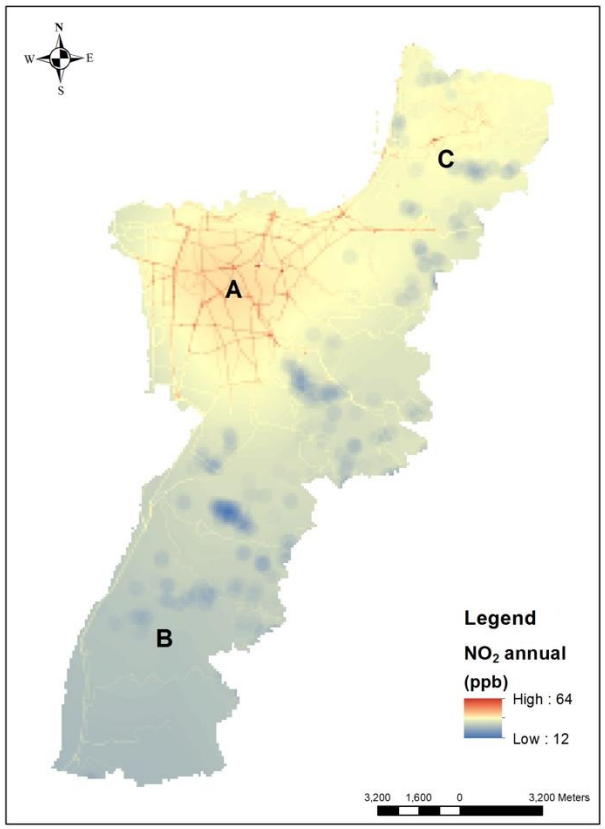

Figure 12. NO_2 annual LUR-based map

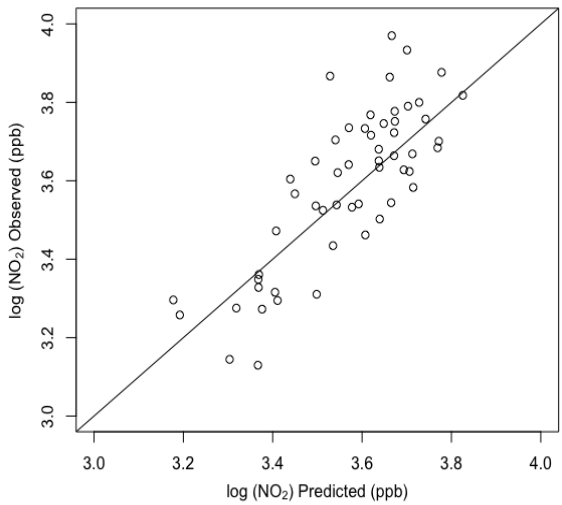

Figure 13. Observed vs predicted annual NO_2 concentrations

3.2.1.2 NO_2 hot-season model

The hot-season NO_2 LUR model was found to be similar to the annual model with respect to its significant predictors (Table 8).

The concentrations of NO_2 during the hot season were found to be positively correlated with building footprint within a 3-km buffer and negatively correlated with the other model predictors that included distance to major roads, distance to the Zouk power plant, relative humidity, low urban area in 300-m buffer, and open areas within a 3-km buffer (Table 8).

Based on the model results, one can conclude that the distance to major roads played a key role in modulating the levels of NO_2 in the hot season. On average, as the distance between a site and its nearest major road increased by 1-km, the NO_2 levels were expected to drop by 16 % on average. The predictive LUR surface map for NO_2 showed patterns similar to the annual averaged NO_2 map; yet the hot-season averaged NO_2 concentrations in the immediate vicinity of major roads were found to be higher than their counterparts in the annual model and the concentrations appear to be more spatially dispersed as can be seen in Figure 14 (Region A). Moreover, the area in the vicinity of the Zouk power plant appears to show higher levels of NO_2 concentrations as compared to the annual map. Overall, the model explained 66% of the variability observed in the hot-season NO_2 concentrations ($R^2 = 0.66$; adjusted $R^2 = 0.62$). The model showed a minor tendency to over-prediction with a PBIAS value of 4%. The RMSE of the model was found to be 0.13. When computing the Moran's I spatial auto-correlation index for the model residuals, the results showed that the model's residuals were generally randomly distributed with no

spatial auto-correlation (Moran's I = 0.0298 and the z-score = -0.55). The 4-fold cross validation results show that the model is robust with a MSPE of 0.0449.

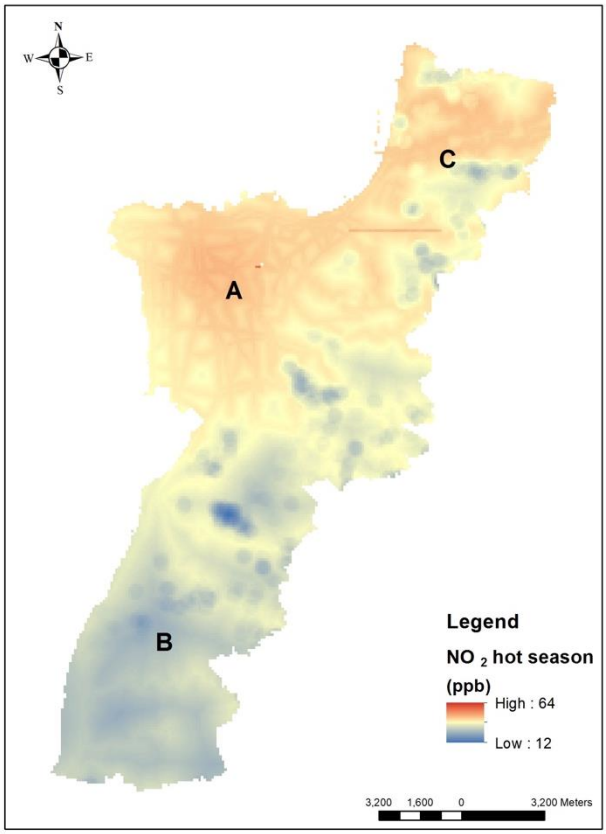

Figure 14. Hot season NO_2 LUR map

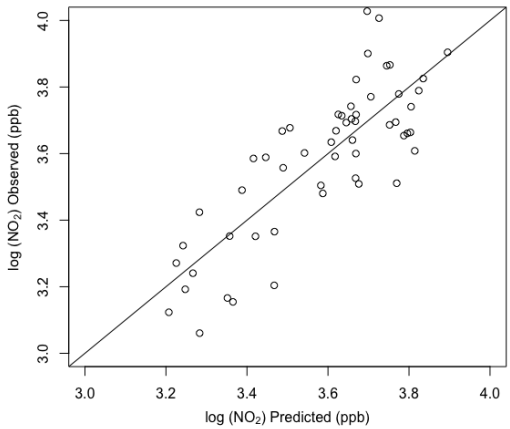

Figure 15. Observed vs predicted NO_2 concentration in the hot season

3.2.1.3 NO2 cold season model

During the cold season, meteorological parameters were found to play an important role in modulating the measured NO_2 levels across sites. Both wind speed and ambient temperatures were found to be significant predictors of NO_2 concentrations in the cold season. Sites that experienced higher wind speeds were found to have lower NO_2 levels, which highlights that role that wind plays in dispersing emissions. However, sites with higher temperatures were found to have on average higher NO_2 levels. This is due to increased formation of NO_2 levels at higher temperatures. Given that NO_2 is a traffic related pollutant, the increase in the length of highways within a 50 meters radius of the sampling sites was found to positively correlate with the measured NO_2 levels. As a matter of fact, for every 100 m increase in the length of highways within a 50 m buffer of a sampling site, the concentration of NO_2 increased on average by around 7%. The effect of the emissions of the Zouk power plant on the NO_2 levels was also very apparent. As can be seen from the model, the measured NO_2 levels were found to drop with distance away from the plant; the model results indicate that the concentrations tended to drop on average by around 11 percent for every 10 km increase in distance. Similar to the annual and the hot season models, areas with a higher percentage of low urban density developments showed on average lower NO_2 levels as compared to similar sites with more dense urbanization. As can be seen in the generated prediction surface, the highest concentrations were expected to be found in the vicinity of highways and major roads as well as in the vicinity of the Zouk power plant (region C). The lowest concentrations were expected in the southern part of the GBA (Region B in Figure 16). In summary, the model explains 73% of the observed

variability in the data and had a low RMSE (0.10) (Figure 17). The model showed a slight tendency to over-predict NO_2 concentrations given that the PBIAS was 4%. In terms of the spatial auto-correlation of the model residuals, Moran's I was found to be equal to 0.007 with a z-score of 0.43, indicating a random spatial distribution of the errors with no clustering in the model residuals. The robustness of the model was also tested using the 4-fold cross-validation. The MSPE value was 0.0442, indicating a strong ability for the model to predict NO_2 concentrations in the cold season.

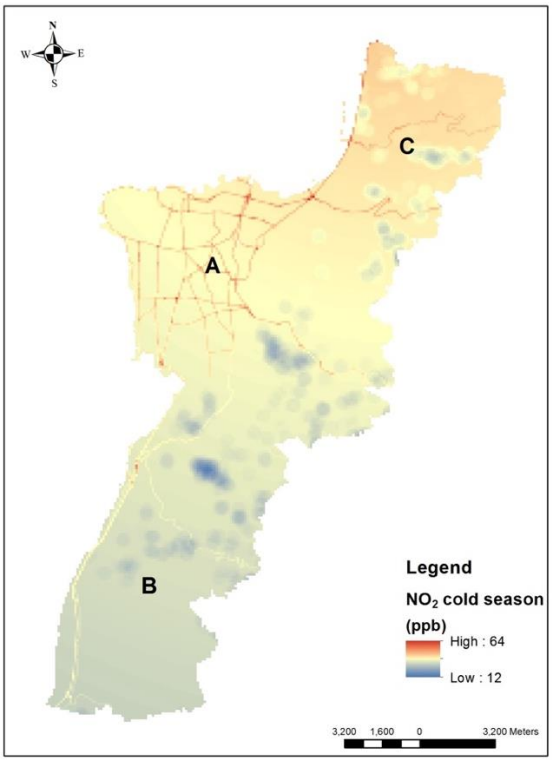

Figure 16. Cold season NO_2 LUR map

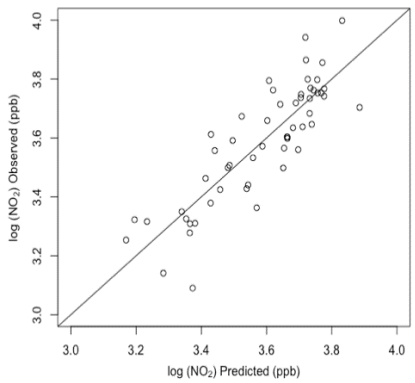

Figure 17. Observed vs predicted NO_2 cold concentrations

3.2.2 NO_x land-use regression models

The LUR models for predicting the annually-averaged NO_x concentrations as well as the seasonal concentrations are summarized in Table 9. The three models were found to share three common predictors namely, the distance to major roads, percent of low urban areas, and the total length of highways within a 50-m buffer. As can be seen in Table 9, most of the significant predictors associated with the NO_2 models were also found to be equally significant for predicting NO_x levels. Similar to the NO_2 models, the traffic-related predictor were found to be positively correlated with the NO_x concentrations, which further highlights the importance of the transport sector in aggravating air pollution within the GBA.

Table 9. LUR models of NOx

	Predictors	Coefficients	t-value	p-value	R^2 Adjusted R^2	RMSE
Annual model: $\log(NO_x)$	(Intercept) highway_50 (km) LUrban_300 (%) MUrban_3000 (%) Building_3000 (%) Distance_major (km)	3.8893 1.5695 -3.1530×10^{-2} 1.42093×10^{-2} 1.19485×10^{-2} -6.169×10^{-1}	26.606 2.392 -2.142 3.200 3.849 -3.086	$< 2\times10^{-16}$ 0.020629 0.037199 0.002409 0.000344 0.003332	0.5724; 0.5288	0.29
Hot season model: $\log(NO_x$ hot)	(Intercept) Building_3000 (%) Distance_Major (km) LUrban_300 (%) Distance_Zouk (km) Highway_50 (km) Wind_speed (kph)	4.4860 1.032×10^{-2} -5.350×10^{-4} -2.771×10^{-2} -1.335×10^{-5} 1.4930 -3.885×10^{-2}	23.516 2.734 -2.809 -1.933 -1.990 2.377 -1.917	$< 2\times10^{-16}$ 0.00873 0.00716 0.05908 0.05231 0.02149 0.06115	0.5973; 0.547	0.28
Cold season model: $\log(NO_x$ cold)	(Intercept) Distance_Zouk (km) Highway_50 (km) LUrban_300 (%) Distance_Major (km) Water_1000 (%)	4.8780 -2.642×10^{-2} 1.9070 -3.202×10^{-2} -6.092×10^{-1} -1.120×10^{-2}	45.858 -4.295 2.708 -2.123 -3.028 -2.219	$< 2 \times 10^{-16}$ 8.25×10^{-5} 0.00930 0.03879 0.00392 0.03112	0.5633; 0.5188	0.30

MUrban_300: Percent area occupied by medium urban areas within a 300m buffer
Water_1000: Percent coverage of waterbodies within a 1 km buffer

3.2.2.1 NO_x annual model

Similar to the NO_2 annual model, the model for the annual NO_x levels had a strong correlation to the traffic related emission predictors, namely distance to highways as well as the length of highways within a 50-meter buffer of a site. Yet unlike the NO_2 model, there was no statistically significant correlation with the Zouk Power plant, the major point source emitter in the GBA. The total length of highways within a 50-m buffer was found to positively correlate with the measured annual NO_x concentrations. As a matter of fact for every 100 m increase in the length of highways within the buffer area, the NO_x levels were expected to increase on average by 17%. On the other hand as the distance separating a site

from the nearest major road increased, the pollution levels were expected to drop. The drop on average was by more than 27% for every 500 m increase in the separation distance. The impact of urbanization was also very clear, sites with a higher percentage of medium urban density tended to have higher NO_x ambient concentrations as compared to areas with a low urban density. Furthermore, the total buildings footprint around a site was found to be positively correlated with the measured NO_x levels. As the percentage of the area covered by buildings within a 3000 m buffer from a site increased by 1 %, the NO_x levels were expected to increase by 1.2% on average. Examining the generated LUR predictive map for the annual NO_x levels in the GBA shows clearly that the highest concentrations tend to occur in the immediate vicinity of the major roads and highways (e.g. Region A in Figure 18). Similarly to NO_2, the highest concentrations tend to be more pronounced within Beirut city, while the lowest concentrations tend to occur in the southern part of the GBA (Region B in Figure 18). Overall, the annual NO_x model was able to explain 57% of the variability observed in the annually averaged NO_x concentrations ($R^2 = 0.57$), with an adjusted R^2 of 0.53. The model displayed a minor tendency to over-predict, with a PBIAS of 3.5%; yet its root mean square error was low (0.29). The Moran's I index based on the model residuals was found to be -0.043 with a z-score of -0.101. This indicates the absence of clustering in the model's residuals. The 4-fold cross-validation had an MSPE of 0.118, showing that the model has a good ability to reproduce results close to the averaged measured NOx annual concentrations.

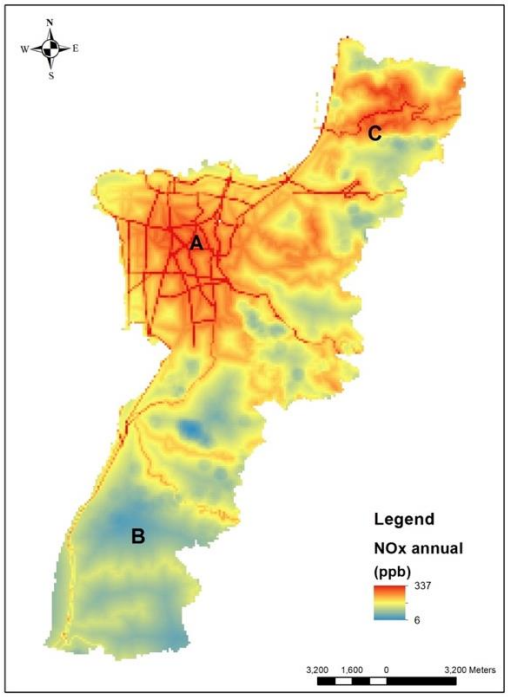

Figure 18. Annual NOx LUR map

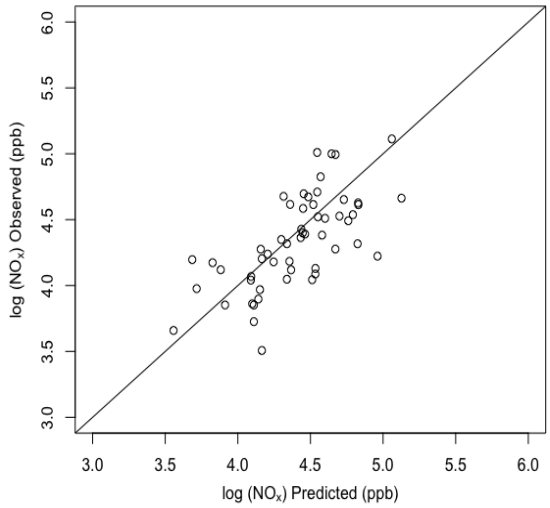

Figure 19. Observed vs Predicted NOx annual concentrations

3.2.2.2 NO_x hot season model

Similar to the annual NO_x model, NO_x concentrations in the hot season were highly correlated with traffic related predictors. In fact, the NO_x levels tended to increase on average by 16% for every additional 100 m of highways within a 50 meter buffer

around a site. Concentrations also tended to decrease as the distance to major roads increased; yet the rate of decrease was much less pronounced as compared to the annual model. This could indicate that NO_x levels in the hot season tend to persist longer around major highways. Unlike the annual model, the effect of the Zouk power plant, the main point source air pollution emitter in the GBA, was found to be statistically significant; yet its magnitude was small and thus insignificant. This is apparent in the generated predictive maps that do not show a local hot-zone in the vicinity of the Zouk power plant. In addition, the NO_x levels in the hot season were found to increase with the increasing footprint of the build-up areas within a 3-km buffer of the sampling sites. A 10 % increase in the build-up footprint tended to increase the NO_x levels by around 11% on average in the hot season. Concentrations were also expected to be lower at sites with higher wind speeds. The generated predictive map clearly shows that the highest NO_x concentrations tended to fall in the immediate vicinity of highways and close to the Zouk power plant as shown in Figure 20. In fact, at the northern extremity of area C lies. Given that the most prominent direction of wind is south western, pollutants tend to accumulate in that area, and show high concentrations since winds carry over the pollutant. On the other hand, the lowest concentrations occur in the southern section of the GBA (Region B). Overall, the predictive LUR-based pollution map for the hot season was found to be very similar to that generated for NO_2 in the same season. This is expected given that the correlation factor between NO_x and NO_2 in the hot season was 0.87 (Table 11). Overall, the model was able to explain 59% of the observed variability in the NO_x concentrations in the hot-season (R^2 = 0.59; adjusted R^2 of 0.55). The model was found to show a slight bias towards over-prediction with a PBIAS value of 5%. The root mean square error of the model was low with a value of 0.30.

Moreover, the model's residuals did not show any statistically significant spatial auto-correlation, whereby the Moran's I index was found to be 0.0273 with a z-score of 0.413. The robustness of the model was assessed with a 4-fold cross-validation, the MSPE was found to have a value of 0.103, which indicates good predictive abilities and lack of over-fitting.

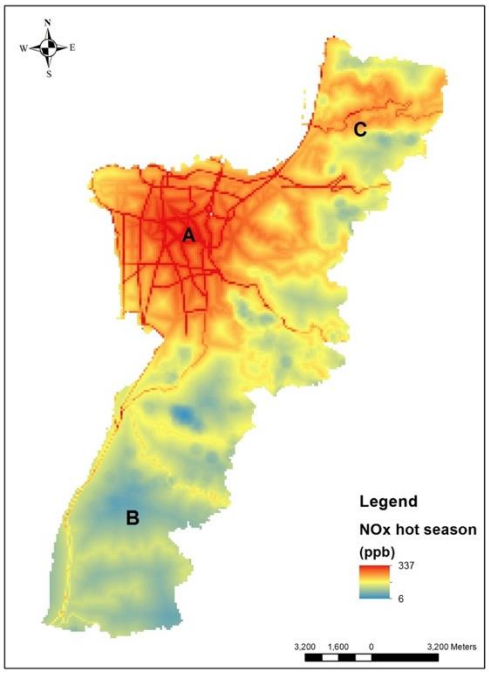

Figure 20. Hot season NOx LUR map

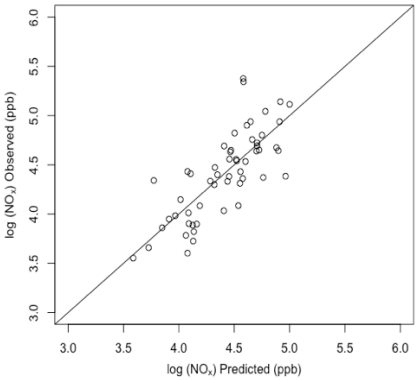

Figure 21. Observed vs predicted NOx concentrations in the hot season

3.2.2.3 NO_x cold season model

The NO_x model for the cold season was found to be largely similar in structure to both the annual and the hot season models; yet it included the percentage of waterbodies within a 1-km buffer as an additional predictor. The correlation between the cold-season NO_x levels and the percentage of water bodies around a given site was found to be negative. On average for every 10 % increase in the percent water coverage a site had, its NO_x levels were expected to decrease by around 11%. The contribution of the Zouk power plant to the cold-season NO_x levels was much more apparent than in the hot season. The concentrations were expected to drop by around 3% per km moving away from the facility. Overall, the highest cold season NO_x levels were expected to be found along highways. Lower values were predicted to be found towards the southern region of the GBA, as shown in Figure 22. Note that coastal regions tended to have lower concentrations as compared to their corresponding hot season concentrations due to the ameliorating effect of nearby water surfaces. Overall, the cold-season model was able to explain 56% of the variability observed in the NO_x concentration ($R^2 = 0.56$) during that season, with an adjusted R^2 of 0.51. This model also had a minor tendency to over-predict concentrations, with a PBIAS value of 0.06. Moreover, the generated predictions were robust with a MSPE value of 0.109. The spatial autocorrelation of the residuals was assessed using the Moran's I metric, which was found to be -0.0018, with a z-score of 0.039. This implies that the model residuals are not clustered but rather have a spatial distribution that can be supported by a completely random spatial process.

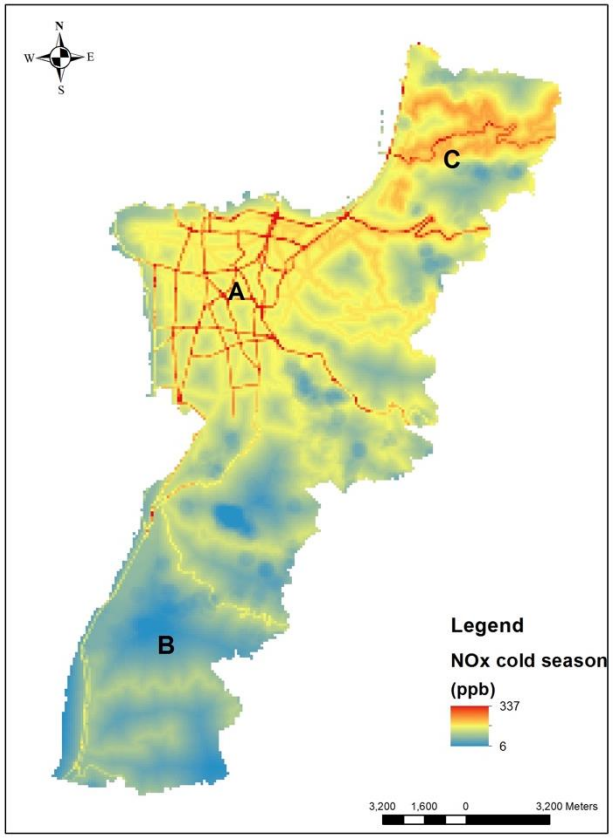

Figure 22. Cold season NOx LUR map

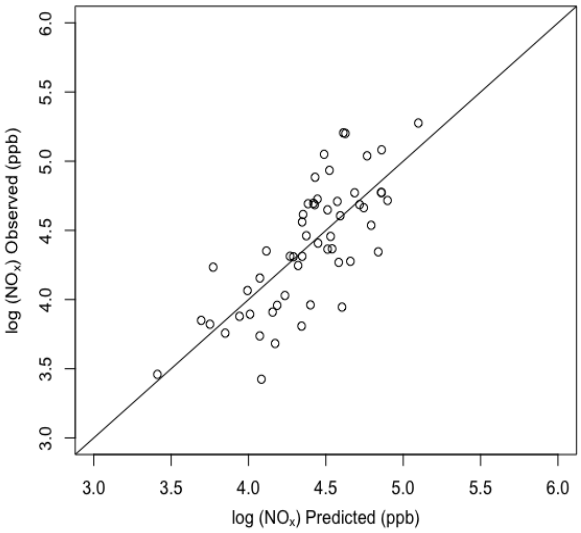

Figure 23. Observed vs predicted NOx cold-season concentrations

3.2.3 O_3 land-use regression models

The LUR models developed to predict O_3 levels at the annual as well as the seasonal levels are summarized in Table 10. All models were found to share one common predictor, namely the percent area occupied by industrial establishments within a 50-m buffer from a given site. Interestingly, this predictor did not feature in any of the NO_2 and NO_x models.

Table 10. LUR models of O_3 annual, hot and cold seasons

	Predictors	Coefficients	t-value	p-value	R^2; adjusted R^2	RMSE
Annual model: log(O_3)	(Intercept) all_roads_3000 (km) Wind_speed (kph) Major_200 (km) Open_2000 (%) Ind_3000 – Ind_50 (%) Ind_50 (%)	3.295 -4.301×10^{-4} 1.700×10^{-2} -6.624×10^{-2} 4.521×10^{-3} -6.087×10^{-3} -7.199×10^{-3}	86.393 -5.574 5.296 -3.411 2.355 -2.247 -2.664	$< 2\times10^{-16}$ 1.12×10^{-6} 2.92×10^{-6} 0.00132 0.02267 0.02925 0.01048	0.6456; 0.6013	0.07
Hot season model: log(O_3 hot)	(Intercept) Water_2000 (%) 1/Distance_Airport (km^{-1}) Open_50 (%) Ind_50 (%) Major_200 (km) Distance_highway (km)	3.33 3.539×10^{-3} -6.446×10^{-1} 1.181×10^{-3} 1.236×10^{-3} -6.993×10^{-2} -3.355×10^{-2}	104.681 4.483 -4.662 1.746 2.181 -3.150 -2.142	$< 2\times10^{-16}$ 4.57×10^{-5} 2.52×10^{-5} 0.04723 0.03413 0.00281 0.03726	0.5426; 0.4854	0.06
Cold season model: log(O_3 cold)	(Intercept) Building_3000 (%) Distance_Zouk (km) All_roads_200 (km) Ind_50 (%) Wind_speed (kph)	3.387 -3.581×10^{-3} 5.384×10^{-3} -4.427×10^{-2} -2.369×10^{-3} 5.435×10^{-3}	54.181 -2.877 2.479 -2.279 -3.002 2.847	$< 2 \times 10^{-16}$ 0.00593 0.01668 0.02707 0.00421 0.000643	0.6095; 0.5697	0.09

All_roads_3000: all roads length in 3km buffer
Water_2000: waterbodies area in 2 km buffer
Major_200: major roads length in 200m buffer
Open_50: Open areas in 50m buffer
Open_2000: open areas in 2km buffer
All_roads_200: all roads length in 200m buffer
Ind_3000: industrial areas in 3 km buffer
Ind_50: industrial areas in 50m buffer

3.2.3.1 O_3 annual model

The annual O_3 model incorporated 4 variables that tended to attenuate O_3 concentrations, these included: the length of roads within a 3-km buffer, the length of major roads within a 200-m buffer, as well as industrial areas within a 50-m buffer and within a 3-km buffer. As can be seen, the aforementioned variables are considered as pollution sources that emit nitrogen oxides. As such, it is suspected that sites with high values of these predictors tend to have a low VOC/NOx ratio, which limit ozone production and accelerate its loss through the NO_x titration process. Overall for every 1 km increase in the total length of major roads within a 200-m buffer, the ozone concentration on average decrease by 6.5%. For the same increase in the total road length within a 3 Km buffer, the expected decrease in ozone concentration was predicted to be marginal. An increase of 10 % in the industrial areas within a 50 m or a 3 Km buffer distance from a site caused the ozone levels to drop on average by 7% and 6% respectively. On the other hand, increases in wind speeds and the percentage of open areas within 2 km of a site tended to increase the predicted ozone levels. This could be due to the low NO_x concentrations in open areas and the ability of the wind to disperse NO_x. Unlike nitrogen oxides, the generated LUR-based map for the annual averaged O_3 levels showed the lowest concentrations in the vicinity of major highways and roads, while the highest levels were expected to be found in the southern region of the GBA as shown in Figure 24. Overall, the annual ozone model was able to explain 64% of the variability observed in the annual O_3 concentrations ($R^2 = 0.64$), with an adjusted R^2 of 0.60. The model had a slight tendency to over-predict concentrations, with a PBIS value of 3%. The RMSE was 0.07, indicating a small deviation between the observed and predicted values. Moreover, there was no

statistically significant spatial autocorrelation in the model residuals (Moran's I metric was -0.0176 with a z-score of -0.296 with a p-value = 0.22). This implies that the model residuals do not show any signs of clustering but rather they tend to have a spatial distribution that can be supported by a completely random spatial process.

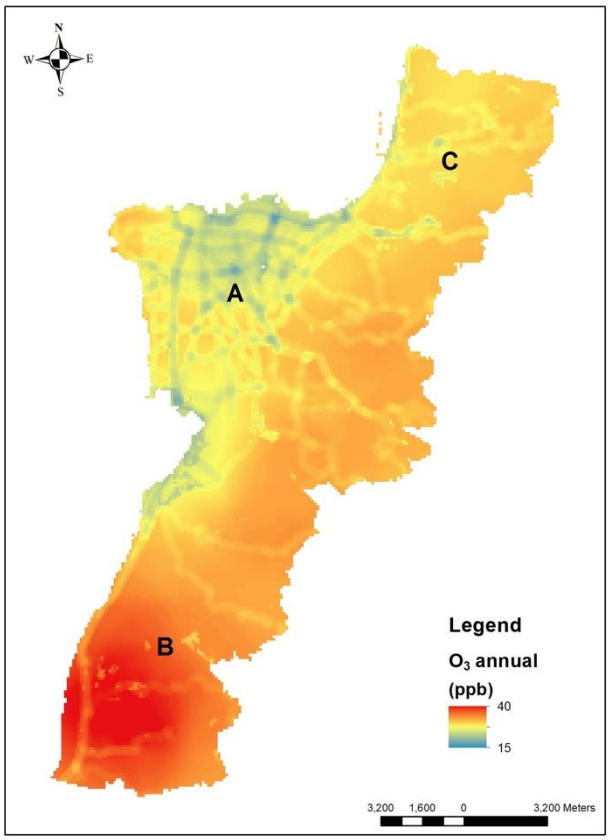

Figure 24. Annual concentrations O_3 LUR map

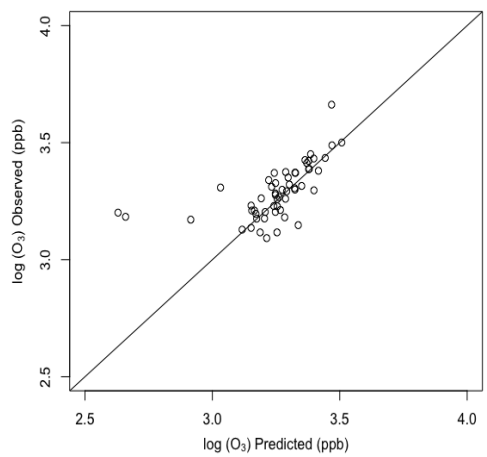

Figure 25. Observed vs predicted O_3 annual concentrations

3.2.3.2 O_3 hot season model

Three significant predictors were found to positively correlate with the measured O_3 levels in the hot season. These included the percentage of waterbodies within a 2-km buffer, open areas within a 50-m buffer, and industrial areas within a 50-m buffer. For every 10 percent increase in these three predictors, the O_3 levels were expected to increase on average by 3.6%, 1.2%, and 1.2% respectively. The length of major roads within a 200-m buffer, distance to highway, and the inverse distance to the airport were found to negatively correlate with the measured O_3 concentrations. As a matter of fact for every 1 km increase in the length of major roads within a 200-m buffer of a site, the ozone levels were expected to drop by around 7%. Ozone concentrations were expected to drop by around 3 % for every 1 km increase in the distance separating a site from the nearest highway. As for the distance to airport, O_3 levels 1 km away from the airport were expected to be on average 27.6% lower than levels 2 km away from the airport. This highlight the potential dominance of low VOC/NO_x environments near major roads and in the vicinity of the airport and thus one would expect that ozone levels decrease as a result of the elevated nitrogen oxides concentrations in these regions. As can be seen from the

predicted median hot-season O_3 concentration map for the GBA, the O_3 concentrations tended to be more spatially homogeneous and lower than the annual average concentrations throughout the whole area. The lowest concentrations appear to be collocated near the major roads, mainly due to the scavenging effect caused by the higher concentrations of nitrogen dioxide (Figure 26). Higher O_3 concentrations in the hot season appear along parts of the shoreline, where the NO_x concentrations were also predicted to be low. Overall, the hot seasonal model for O_3 in the GBA was able to explain only 54% of the variability in the observed concentrations ($R^2 = 0.54$) with an adjusted R^2 of 0.48. Moreover, the RMSE value was found to be 0.06. The model had a slight tendency to over-predict concentrations, with a PBIAS value of 0.11%. No spatial auto-correlation was observed for the residuals (Moran's I = -0.0473; z-score = -0.521, p-value = 0.23). The hot season model proved to be robust, with a MSPE value of 0.0639.

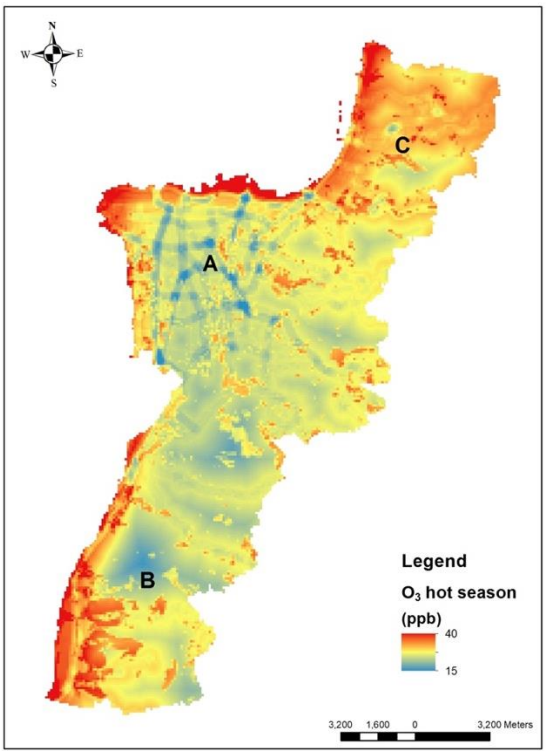

Figure 26. Hot concentrations O_3 LUR map

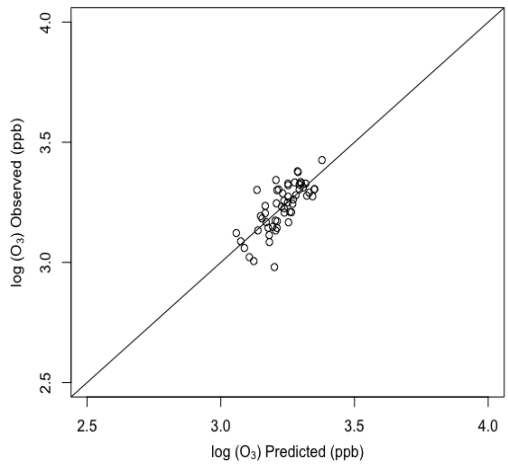

Figure 27. Observed vs predicted O_3 hot-season concentrations

3.2.3.3 O_3 cold season model

In the cold season, increases in the building footprints within a 3-km buffer of a site, the length of roads within a 200-m buffer, and the percent area that is industrial within a 50-m buffer of a site were all found to correlate negatively with the measured O_3 concentrations. Interestingly, these variables were positively associated with the NO_2 and NO_x concentrations in the cold season; this further emphasizes that in the more urban areas of the GBA the scavenging of ozone by NO_x exceeds its generation rate thus hinting to the presence of a low VOC/NOx ratio in these zones. Ozone concentrations in the cold season tended to increase with increasing distance from the Zouk power plant and with increased wind speeds. Spatially, the cold-season LUR-based map was similar to the one generated for the annually averaged concentrations. As can be seen in Figure 28, the lowest concentrations are found next to roads. On the other hand, the highest levels were found in the low urban southern section of the GBA (region B in Figure 28). Overall, the cold season ozone model explained 60% of the variability observed in the measured

concentrations (R^2 = 0.60), with an adjusted R^2 of 0.56. The model had a slight tendency to over-predict with a PBIS value of 3%. No spatial autocorrelation was observed in the model residuals (Moran's I index = -0.0102; z-score = 0.32, p-value = 0.19). The MSPE value was 0.0327 indicating a robust model.

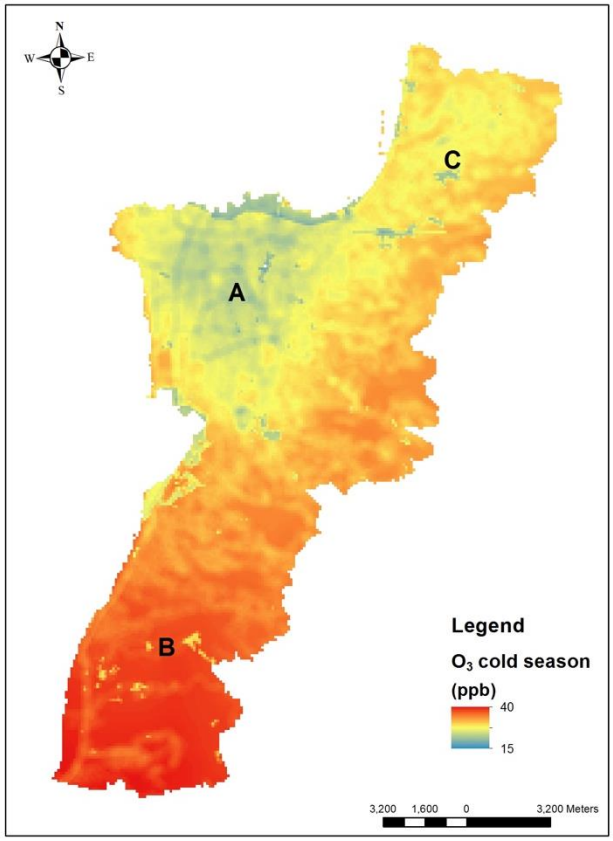

Figure 28. Cold season O_3 LUR map

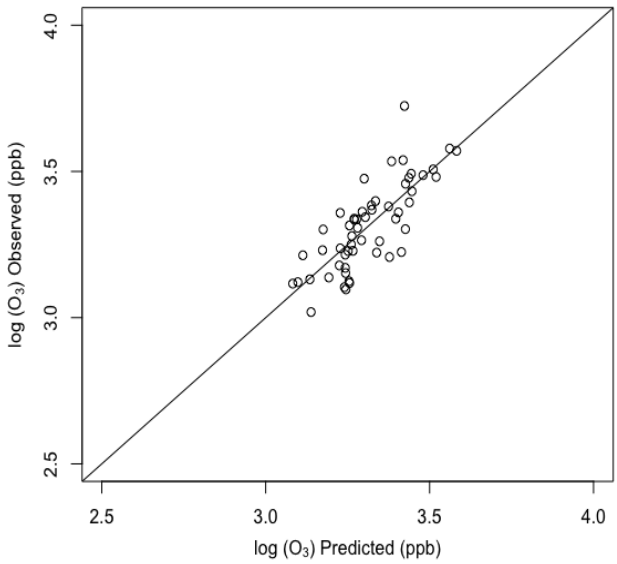

Figure 29. Observed vs predicted cold-season O_3 concentrations

3.3 Correlation between the pollutants

The correlations between the predicted NO_2 and NO_x concentrations for the annual, hot, and cold season were found to be higher than the correlations associated with the measured concentrations(annual r=0.86 vs 0.70; hot season r=0.87 vs 0.80; cold season r= 0.83 vs 0.67). This could be an artifact of the high similarity in model structure between the NO_2 and NO_x LUR models. The correlation between the predicted NO_2 and O_3 surfaces was found to be negative and high for the annual and cold season, reaching -0.78 and -0.73 respectively. These correlations were largely similar to those associated with the correlation observed for the measured levels (-0.7 for both annual and cold season). During the hot season, the correlation between the two pollutants proved to be weak and not significant (correlation factor of -0.08). Field-based hot season correlation was also negative but was higher in magnitude (r = -0.21). Similar to the case of NO_2, the correlation between NO_x and O_3 was also negative and high for the annual and winter

models (correlation = -0.70 and -0.71 respectively, p-value < 2.2×10^{-6}). This relationship was also found to weaken in the hot season, where the correlation factor dropped to -0.12. Correlations based on the field-measurements were largely similar across seasons and for the annually averaged levels.

Table 11. Correlation matrix between the generated pollutant prediction maps

		NO_2	NOx	O_3
Annual	NO_2	1.00	0.86	-0.78
	NOx	0.86	1.00	-0.70
	O_3	-0.78	-0.70	1.00
Cold	NO_2	1.00	0.83	-0.73
	NOx	0.83	1.00	-0.71
	O_3	-0.73	-0.71	1.00
Hot	NO_2	1.00	0.87	-0.08
	NOx	0.87	1.00	-0.12
	O_3	-0.08	-0.12	1.00

CHAPTER 4
DISCUSSION & CONCLUSION

4.1 Pollutant variability

The adopted sampling campaign extended between August 2017 and July 2018, inclusive. The data collected in this campaign is the most extensive for the GBA to date given its spatial representativeness (around 0.25 sites per km^2) and its extended sampling period. The measured levels of nitrogen dioxides across the monitoring sites varied between 14.7 and 67.9 ppb with a mean of 36.87 ppb. Previous monitoring studies conducted in Beirut city proper had reported that NO_2 varied between 0.1 and 73 ppb (Farah et al., 2014), while Badaro-Saliba et al. (2014) reported that levels fluctuated between 18 and 34.04 ppb. When compared to other cities, specifically the 36 European cities in the ESCAPE project, the GBA measured concentrations exceeded all reported levels. Additionally, the annually averaged GBA levels were found to exceed levels reported in Taipei, Taiwan, Shizuoka, Japan, and Ulaanbaatar, Mongolia (Kashima et al, 2019; Huang et al., 2013; Lee et al., 2014). Overall, the annually averaged concentrations in the GBA were all found to exceed the WHO annual standard set for NO_2 but did not exceed the annual standards set by the USEPA nor the MoE. These levels can be considered as a potential public health concern and thus will necessitate the implementation of more stringent air quality emission controls in Lebanon. As it happens, epidemiological studies have shown that concentrations lower than the set standards by the WHO (lower than our measured concentrations too) have been linked to different respiratory diseases and death across several cities (Ackermann-Liebrich, Felber Dietrich, & Joss, 2019;

Casquero-Vera et al., 2019; Castro, Künzli, & Götschi, 2017; Chaloulakou, Mavroidis, & Gavriil, 2008; Keuken, Roemer, Zandveld, Verbeek, & Velders, 2012).

Seasonal patterns in our study have shown higher concentrations during the cold season when compared to the hot season's concentrations, as is the case in many other studies (Bozkurt, Üzmez, Döğeroğlu, Artun, & Gaga, 2018; Gibson et al., 2013; Hargreaves et al., 2000; Kasparoglu, Incecik, & Topcu, 2018; Mahajan et al., 2015). Cold season averaged concentrations in the GBA were found to vary between 21.99 and 54.54 ppb with an average of 36.75 ppb. These levels are higher than those reported in a study conducted in nearby Marmara, Turkey, where winter mean concentrations recorded at 7 urban sites varied between 14 and 28.8 ppb (Kasparoglu et al., 2018). Interestingly, the winter NO_2 levels in Beirut were also found to be higher than those reported in the much larger and industrialized city of Chengdu, China (winter mean level = 31.38 ppb) (Zhu et al., 2019). In the summer, GBA averaged NO_2 levels were found to exceed even more the mean concentrations reported in Chengdu (22.8 ppb) and in Marmara (5.26 to 18.3 ppb).

Concentrations of NO_x followed closely NO_2 levels as expected given the high correlation observed between the two pollutants. The NO_x levels in the GBA ranged between 25.6 and 270.0 ppb, with a mean of 89.70 ppb. These values were found to be higher than those reported across the 36 European cities in the ESCAPE project, where NO_x concentrations were found to vary between 0.3 ppb and 148.9 ppb. Moreover, the mean GBA NO_x levels were found to significantly excee levels recorded in Augsburg – Germany, where NO_x was found to vary between a minimum of 7.6 and a maximum of 23 ppb (Wolf et al., 2017), and in Taipei-Taiwan, where the average NO_x level was found to be 34.4 ppb. In Metropolitan Perth, Western Australia, Dirgawati et al. (2015) reported

even lower NO_x concentrations with summer averaged concentrations of 2.82 ppb and winter averaged levels of 6.43 ppb. Seasonally, NO_2 and NO_x levels were generally higher during the cold season as reported is other studies (Gibson et al., 2013; Hargreaves et al., 2000; Mahajan et al., 2015). Yet the seasonal differences in their concentrations was relatively low.

With respect to the ozone levels, the GBA measured concentrations were found to vary between 15.76 and 49.10 pbb, with a mean of 26.9 ppb. These values are largely higher that what has been previously reported across Lebanon (O_3 varied between 1.1 and 37.9 ppb, with a mean level of 24.9 ppb) (Abdallah et al., 2016; Farah et al., 2014; Saliba et al., 2006). In comparison to levels reported in some European cities, the GBA O_3 levels were significantly lower (Beelen, Hoek, Vienneau, Eeftens, Dimakopoulou, Pedeli, Tsai, Künzli, Schikowski, Marcon, Eriksen, et al., 2013; Kerckhoffs et al., 2015). When comparing seasonal concentrations, our measured ozone levels showed a strong seasonal signal. Interestingly, ozone concentrations were found to be higher in the cold season as compared to the hot season, especially in the southern low urban areas of the GBA. This seasonal variability in ozone was unexpected given that ozone is a well-known summer pollutant (Bhardwaj et al., 2018; Mahata et al., 2018; Wang et al., 2018). Yet, the winter of 2017-2018 was exceptionally mild with average monthly temperatures ranging between 17 and 25 ^{o}C. The annually averaged concentrations were found to be below the set environmental standards. Nonetheless, ozone standards are only defined in terms of an 8 hour exposure period.

4.2 LUR models

Annual and seasonal LUR models were developed to predict the spatial variability of NO_2, NO_x, and O_3 levels within the GBA. The calibrated models were then employed to generate pollution surfaces for the GBA. In summary, the model predictions showed similar patterns of behavior for both NO_2 and NO_x. The O_3 pollution surface was found to be negatively correlated with the surface of the two other pollutants. In addition, most point sources and traffic related predictors tended to have small buffers when compared to urbanization and landuse predictors. This highlights the effect of the plume dispersion from point sources and vehicular movement allowing for the pollutants to spread, reaching urbanized areas. Urbanized areas and other landuse covers tend to cluster the pollutants and receive the plumes of point sources, thus having a higher buffer enclosing the different effect of pollution.

Nitrogen oxides (including nitrogen dioxide) are known traffic-related pollutants and as such their levels were expected to peak next to major roads. In our models, traffic-related predictors were found to be highly significant across all the annual and seasonal NO_2 and NO_x models. These variables included distance to major roads within 50m buffer, distance to major roads, and distance to highways within 50 m buffer. Both road length and distance away from roads have been found to be common predictors across many NO_2 and NO_x models (Beelen, Hoek, Vienneau, Eeftens, Dimakopoulou, Pedeli, Tsai, Künzli, Schikowski, Marcon, Eriksen, et al., 2013; Cordioli et al., 2017; de Hoogh et al., 2018; Huang et al., 2017; Lee et al., 2014; Rahman et al., 2017). Moreover, the building area within a 3000 m buffer also proved to be a common predictor across the NO_2 and NO_x LUR models. The building area was found to be highly correlated with the total length of

roads and the length of major roads within the same buffer; thus it also acts as a surrogate for traffic-related emissions in dense urban areas. Moreover, this predictor is a proxy of emissions resulting from the use of private diesel generators, whose numbers are expected to be directly proportional to building density. The R^2 of the annual GBA LUR models for NO_2 and NO_x were 0.68 and 0.57, respectively. Thus the performance of the GBA models were largely within the range reported in the ESCAPE project, where the R^2 for the NO_2 LUR models developed for 36 European cities ranged between 55% and 92%, with a median of 82%, while the performance of the NO_x LUR models was slightly lower and ranged between 49 and 91% (Beelen, Hoek, Vienneau, Eeftens, Dimakopoulou, Pedeli, Tsai, Künzli, Schikowski, Marcon, & others, 2013). Moreover, model performance of the GBA models was similar or slightly better than those reported for several other Asian cities such as Shizuoja-Japan, Taipei-Taiwan, Tianhin-China, and Ulaanbaatar-Mongolia (Lee et al., 2014; Huang et al., 2013; Chen et al., 2010; Kashima et al., 2009). It should be stated that including the total number of vehicles as an additional predictor was able to increase the predictive power of all six NO_2 and NO_x models, with some models showing an increase in the R^2 up to 81%. Note that traffic counts have been often used for predicting NO_2 and NO_x levels in several LUR modeling studies (Beelen, Hoek, Vienneau, Eeftens, Dimakopoulou, Pedeli, Tsai, Künzli, Schikowski, Marcon, & others, 2013; Cyrys et al., 2012; Dirgawati et al., 2015; Liu et al., 2015; Rahman et al., 2017). The decision to exclude traffic counts from the final GBA models was due to the lack of accurate traffic data at the level of the GBA.

In addition to the traffic related predictors, all six NO_2 and NO_x models shared a set of common predictors, which highlighting the strong association between the two

pollutants. The common predictors included the area of buildings within a 3-km buffer, the low urban areas within 300-m buffer, and the distance to Zouk power plant. These findings highlight the important role that the Zouk power plant has on pollution levels in the GBA. The polluting effect of the power plant on its surrounding area is well known and has been described by several studies (Azar, 2018; Nassar, 2016; Salloum et al., 2018; Weatherbee, 2015). Nevertheless, since the power plant is located at the far northern edge of the study area it is difficult to distinguish between the direct effect of the plant versus its location acting as a latent variable for the transport of air pollution northwards due to the prevailing southwesterly dominant winds. Meteorological factors were also found to play an important role in modulating the spatial distribution of the NO_2 and NO_x surfaces. The results show that for the hot and annual models, increases in the relative humidity negatively correlated with the predicated NO_2 levels. This was largely attributed to the enhanced removal of NO_2 from the atmosphere under such conditions (Valuntaitė et al., 2012). On the other hand, it was found that increases in wind speed and temperature, especially in the cold model, resulted in a decrease in the predicted NO_2 and NO_x levels. Increases in wind speeds permit for the better dispersion of pollutant emissions. The similarity in model structure between the annual and the seasonal models as well as the high correlations between their respective predictive surfaces further reinforces the absence of significant seasonal differences in their sources and sinks at the GBA level.

With regards to the O_3 LURs, large differences were found between the annual and seasonal model both in terms of model structure and the generated prediction surfaces. We think that this is a due to the competing pathways of ozone generation and destruction as well as to the natural fluctuations in the ambient environmental, which control the

generation and removal of the pollutant near the surface. The levels of O_3 are well known to vary as a function of the meteorological conditions, atmospheric chemistry, as well as the VOC to NO_x ratio. This ratio and its impact on ambient O_3 levels has been studied since the 1990s (Sillman, 1999). O_3 concentrations have been shown to decrease with increases in the NOx levels, when the VOC/NOx ratio is low; these conditions are described as a VOC sensitive regime. On other hand, under a NOx sensitive regime (high VOC/NOx) O_3 levels are expected to increase with increases in NOx. These relationships between VOC, NO_x and O_3 have been used to describe ozone's diurnal behavior (Yang et al., 2018). In our results, overall the correlation between O_3 and NOx was strongly negative pointing towards a dominance of a low VOC/NOx ratio regime within the GBA. Yet, in the hot summer months this negative correlation weakens and becomes insignificant. This could point to an increase of VOC levels in the GBA or to the changing meteorological conditions that promote the formation of ozone. With respect to the LUR predictors, all ozone models included the percent industrial area within a 50-m buffer as a predictor. Increases in the industrial area coverage resulted in a drop in the predicted ozone levels for the annual and cold model; yet it was associated with an increase in ozone concentrations in the hot model. Usually, industrial areas within the GBA rely heavily on private diesel generators as a result of daily network electricity shortages and thus they are expected to emit high levels of NO_2 and NO_x. As such, a VOC sensitive regimen is expected to be found in the immediate vicinity of these areas and hence the negative correlation with ozone. During the hot season, the presence of sunlight and UV rays appears to favor the net generation of ozone in these areas given the positive coefficient in the hot season. Another important predictor of O_3 was the presence of open area that was found to be a significant predictor in

the annual and hot season models of ozone. Open areas and sites with high wind speeds were found to positively correlate with ozone levels, largely due to the low scavenging of ozone levels by NOx due to enhanced dispersion. Interestingly, the impact of the Beirut International Airport was only significant in the hot season, with sites close to it associated with lower ozone levels. This is to be expected since airports are major sources of NOx. With regards to model performance, the R^2 for the annual LUR model was 0.65, while the performance of the cold and hot LUR models ranged between 0.61 and 0.54 respectively. The performance of O_3 LUR models in several European studies were generally higher with Wolf et al. (2017) reporting an R^2 of 0.91 for Augsburg-Germany, Kerckhoffs et al. (2015) reporting an R^2 of 0.77 for the Netherlands, and de Hoogh et al. (2018) reported an R^2 of 0.677 for a cold season model developed for Western Europe.

4.3 Correlation between pollutants from field measurements and prediction maps

As seen in Table 7 and Table 11 in the results, the correlation factors between the three pollutants prediction surfaces were very similar to those calculated between the measurements. This indicates that the developed LUR were able to preserve the inter-pollutant correlations measured in the field. Overall, the NO_2 and NO_x levels were found to be highly positively correlated, while both showed a negative correlation with O_3. In a study conducted by Kerckhoffs et al. (2015), they reported that the correlation between NO_2 and O_3 was -0.87, which is close to the values observed in the GBA- with the exception of the cold season when the strength of the correlation dropped. This hints at the potential of seasonal decoupling between NOx and ozone in the GBA. In another study, Wolf et al. (2017) reported low correlations between NO_2 and NOx on one hand and O_3 on

the other for the cold season. Their correlations were -0.32 and -0.28 for NO_2 and O_3 and NO_x and O_3 respectively. The correlations they reported between NO_2 and NO_x (r = 0.88) were also high and similar to the ones observed in the GBA.

4.4 Limitations

When comparing our models with other studies, the most important and common predictor that wasn't included in our study was traffic count. Since the pollutants are traffic-related, collecting accurate traffic counts across Beirut appears to be imperative. In addition, generating and including detailed street-level data such as population, building heights, and economic activity in the LUR models is expected to improve model performance. Unfortunately, such information is lacking for the GBA. Another limitation of this study is the inability of the contemporaneous deployment of the OGAWAs measurements across all sites due to the lack of available units. Yet, this impact is expected to be minor given that the deployment was over an entire week. With regards to O_3, the concurrent measurement of VOC levels would have allowed us to better understand and quantify the relationship between O_3 and VOC/NO_x. Other limitations emerge from the laboratory, in terms of the different lab equipment and instruments used.

4.5 Conclusion

Given the low budget allocated for the Ministry of Environment, our study allowed us to cover the sampling gap in the Greater Beirut Area, resolving the spatial coverage issue and tackling the spatio-temporal variability of the different pollutants. LUR annual and seasonal models were developed for NO_2, NO_x and O_3. The models'

development was based on the ESCAPE method and encompassed different types of predictors, but the most important ones were traffic related sources. This study has demonstrated that LUR models can in fact be used as tools to predict or estimate traffic-related air pollutants in the GBA. They can be used as a tool to predict the population's exposure to bad air quality, allowing for the implementation of policies that enhance the public health's welfare. Performance of the models were actually close to the range of already published papers. However, this is the first study that tackles air pollution in Lebanon with an extensive network for monitoring. These models are the first step in assessing exposures in the study area and can be further improved when complementing them with personal exposures to air pollution.

In order to develop a control strategy for air pollution, we still have a long way to go. However, further studies should be conducted in Lebanon to determine the priority pollutants and thus relating them to specific activities. Once this is done, one can identify the measures that need to be taken to control these sources and thus developing a control strategy based on the aforementioned. The control strategy should be enforced and should comply with the different standards set locally and internationally (USEPA, 2018). In fact, this is the major problem in Lebanon. The lack of monitoring and enforcement of the law has allowed different industries and several activities to take place and disturb our air quality. Other management strategies done in polluted countries like Beijin, China, have relied on a hybrid population-production-pollution nexus model to be used for air pollution management and air quality planning (Zeng et al., 2017) which can also be applied later on in Lebanon.

BIBLIOGRAPHY

Abdallah, C., Sartelet, K., & Afif, C. (2016). Influence of boundary conditions and anthropogenic emission inventories on simulated O3 and PM2.5 concentrations over Lebanon. *Atmospheric Pollution Research, 7*(6), 971-979. doi:10.1016/j.apr.2016.06.001

Ackermann-Liebrich, U., Felber Dietrich, D., & Joss, M. K. (2019). Respiratory and Cardiovascular Effects of NO2☆ *Reference Module in Earth Systems and Environmental Sciences*: Elsevier.

Adon, M., Galy-Lacaux, C., Yoboué, V., Delon, C., Lacaux, J. P., Castera, P., . . . Mougin, E. (2010). Long term measurements of sulfur dioxide, nitrogen dioxide, ammonia, nitric acid and ozone in Africa using passive samplers. *Atmos. Chem. Phys., 10*(15), 7467-7487. doi:10.5194/acp-10-7467-2010

Atari, D. O., Luginaah, I., Xu, X., & Fung, K. (2008). Spatial Variability of Ambient Nitrogen Dioxide and Sulfur Dioxide in Sarnia, "Chemical Valley," Ontario, Canada. *Journal of Toxicology and Environmental Health, Part A, 71*(24), 1572-1581. doi:10.1080/15287390802414158

Azar, G. (2018). Jounieh a regional hotspot for pollution, says greenpeace. *Yerepouni Daily News*.

Badaro-Saliba, N., Adjizian-Gerard, J., Zaarour, R., Abboud, M., Farah, W., Saliba, A. N., & Shihadeh, A. (2014). A geostatistical approach for assessing population exposure to NO2 in a complex urban area (Beirut, Lebanon). *Stochastic Environmental Research and Risk Assessment, 28*(3), 467-474. doi:10.1007/s00477-013-0765-3

Beelen, R., Hoek, G., Vienneau, D., Eeftens, M., Dimakopoulou, K., Pedeli, X., . . . de Hoogh, K. (2013). Development of NO2 and NOx land use regression models for estimating air pollution exposure in 36 study areas in Europe – The ESCAPE project. *Atmospheric Environment, 72*, 10-23. doi:https://doi.org/10.1016/j.atmosenv.2013.02.037

Beelen, R., Hoek, G., Vienneau, D., Eeftens, M., Dimakopoulou, K., Pedeli, X., . . . others. (2013). Development of NO 2 and NO x land use regression models for estimating air pollution exposure in 36 study areas in Europe–the ESCAPE project. *Atmospheric Environment, 72*, 10-23.

Berman, J. D., Breysse, P. N., White, R. H., Waugh, D. W., & Curriero, F. C. (2015). Evaluating methods for spatial mapping: Applications for estimating ozone concentrations across the contiguous United States. *Environmental Technology & Innovation, 3*, 1-10. doi:https://doi.org/10.1016/j.eti.2014.10.003

Bhardwaj, P., Naja, M., Rupakheti, M., Lupascu, A., Mues, A., Panday, A. K., . . . Lawrence, M. G. (2018). Variations in surface ozone and carbon monoxide in the Kathmandu Valley

and surrounding broader regions during SusKat-ABC field campaign: role of local and regional sources. *Atmos. Chem. Phys.*, *18*(16), 11949-11971. doi:10.5194/acp-18-11949-2018

Bozkurt, Z., Üzmez, Ö. Ö., Döğeroğlu, T., Artun, G., & Gaga, E. O. (2018). Atmospheric concentrations of SO2, NO2, ozone and VOCs in Düzce, Turkey using passive air samplers: Sources, spatial and seasonal variations and health risk estimation. *Atmospheric Pollution Research*, *9*(6), 1146-1156. doi:https://doi.org/10.1016/j.apr.2018.05.001

Bravo, M. A., Son, J., de Freitas, C. U., Gouveia, N., & Bell, M. L. (2016). Air pollution and mortality in Sao Paulo, Brazil: Effects of multiple pollutants and analysis of susceptible populations. *J Expos Sci Environ Epidemiol*, *26*(2), 150-161. doi:10.1038/jes.2014.90

Brønnum-Hansen, H., Bender, A. M., Andersen, Z. J., Sørensen, J., Bønløkke, J. H., Boshuizen, H., . . . Loft, S. (2018). Assessment of impact of traffic-related air pollution on morbidity and mortality in Copenhagen Municipality and the health gain of reduced exposure. *Environment International*, *121*, 973-980. doi:https://doi.org/10.1016/j.envint.2018.09.050

Bytnerowicz, A., Fenn, M. E., Cisneros, R., Schweizer, D., Burley, J., & Schilling, S. L. (2019). Nitrogenous air pollutants and ozone exposure in the central Sierra Nevada and White Mountains of California – Distribution and evaluation of ecological risks. *Science of The Total Environment*, *654*, 604-615. doi:https://doi.org/10.1016/j.scitotenv.2018.11.011

Cascio, W. E. (2016). Proposed pathophysiologic framework to explain some excess cardiovascular death associated with ambient air particle pollution: Insights for public health translation. *Biochimica et Biophysica Acta (BBA) - General Subjects*, *1860*(12), 2869-2879. doi:https://doi.org/10.1016/j.bbagen.2016.07.016

Casquero-Vera, J. A., Lyamani, H., Titos, G., Borrás, E., Olmo, F. J., & Alados-Arboledas, L. (2019). Impact of primary NO2 emissions at different urban sites exceeding the European NO2 standard limit. *Science of The Total Environment*, *646*, 1117-1125. doi:https://doi.org/10.1016/j.scitotenv.2018.07.360

Castro, A., Künzli, N., & Götschi, T. (2017). Health benefits of a reduction of PM10 and NO2 exposure after implementing a clean air plan in the Agglomeration Lausanne-Morges. *International Journal of Hygiene and Environmental Health*, *220*(5), 829-839. doi:https://doi.org/10.1016/j.ijheh.2017.03.012

Chaloulakou, A., Mavroidis, I., & Gavriil, I. (2008). Compliance with the annual NO2 air quality standard in Athens. Required NOx levels and expected health implications. *Atmospheric Environment*, *42*(3), 454-465. doi:https://doi.org/10.1016/j.atmosenv.2007.09.067

Chen, T.-M., Kuschner, W. G., Gokhale, J., & Shofer, S. (2007). Outdoor Air Pollution: Ozone Health Effects. *The American Journal of the Medical Sciences, 333*(4), 244-248. doi:https://doi.org/10.1097/MAJ.0b013e31803b8e8c

Cordioli, M., Pironi, C., De Munari, E., Marmiroli, N., Lauriola, P., & Ranzi, A. (2017). Combining land use regression models and fixed site monitoring to reconstruct spatiotemporal variability of NO2 concentrations over a wide geographical area. *Science of The Total Environment, 574*, 1075-1084. doi:https://doi.org/10.1016/j.scitotenv.2016.09.089

Cyrys, J., Eeftens, M., Heinrich, J., Ampe, C., Armengaud, A., Beelen, R., . . . Hoek, G. (2012). Variation of NO2 and NOx concentrations between and within 36 European study areas: Results from the ESCAPE study. *Atmospheric Environment, 62*, 374-390. doi:https://doi.org/10.1016/j.atmosenv.2012.07.080

de Hoogh, K., Chen, J., Gulliver, J., Hoffmann, B., Hertel, O., Ketzel, M., . . . Hoek, G. (2018). Spatial PM2.5, NO2, O3 and BC models for Western Europe – Evaluation of spatiotemporal stability. *Environment International, 120*, 81-92. doi:https://doi.org/10.1016/j.envint.2018.07.036

Deville Cavellin, L., Weichenthal, S., Tack, R., Ragettli, M. S., Smargiassi, A., & Hatzopoulou, M. (2016). Investigating the Use Of Portable Air Pollution Sensors to Capture the Spatial Variability Of Traffic-Related Air Pollution. *Environmental Science & Technology, 50*(1), 313-320. doi:10.1021/acs.est.5b04235

Dirgawati, M., Barnes, R., Wheeler, A. J., Arnold, A.-L., McCaul, K. A., Stuart, A. L., . . . Heyworth, J. S. (2015). Development of Land Use Regression models for predicting exposure to NO2 and NOx in Metropolitan Perth, Western Australia. *Environmental Modelling & Software, 74*, 258-267. doi:https://doi.org/10.1016/j.envsoft.2015.07.008

Dirgawati, M., Heyworth, J. S., Wheeler, A. J., McCaul, K. A., Blake, D., Boeyen, J., . . . Hinwood, A. (2016). Development of Land Use Regression models for particulate matter and associated components in a low air pollutant concentration airshed. *Atmospheric Environment, 144*, 69-78. doi:10.1016/j.atmosenv.2016.08.013

Durant, J. L., Beelen, R., Eeftens, M., Meliefste, K., Cyrys, J., Heinrich, J., . . . Hoek, G. (2014). Comparison of ambient airborne PM2.5, PM2.5 absorbance and nitrogen dioxide ratios measured in 1999 and 2009 in three areas in Europe. *Science of The Total Environment, 487*, 290-298. doi:https://doi.org/10.1016/j.scitotenv.2014.04.019

El Khoury, N. A. J., Lea Kai; Kadehjian, Korkin. (2016). Road Transport Sector and Air Pollution: Case of Lebanon 2016.

EPA. (2010). Primary National Ambient Air Quality Standards for Nitrogen Dioxide; Final Rule.

EPA. (2016, September 8, 2016). Nitrogen Dioxide Basics. Retrieved from https://www.epa.gov/no2-pollution/basic-information-about-no2

ESRI. (2018a). How Spatial Autocorrelation (Global Moran's I) works. Retrieved from http://desktop.arcgis.com/en/arcmap/latest/tools/spatial-statistics-toolbox/h-how-spatial-autocorrelation-moran-s-i-spatial-st.htm

ESRI. (2018b). Install the R-ArcGIS bridge and start statistical analysis. Retrieved from https://learn.arcgis.com/en/projects/analyze-crime-using-statistics-and-the-r-arcgis-bridge/lessons/install-the-r-arcgis-bridge-and-start-statistical-analysis.htm

Farah, W., Nakhlé, M. M., Abboud, M., Annesi-Maesano, I., Zaarour, R., Saliba, N., . . . Gerard, J. (2014). Time series analysis of air pollutants in Beirut, Lebanon. *Environmental Monitoring and Assessment, 186*(12), 8203-8213. doi:10.1007/s10661-014-3998-9

Fox, J., & Weisberg, S. (2011). *An R Companion to Applied Regression* (2nd ed.). Thousands Oak, CA: SAGE Publications.

Getis, A., & Ord, J. K. (1992). The Analysis of Spatial Association by Use of Distance Statistics. *Geographical Analysis, 24*(3), 189.

Gibson, M. D., Heal, M. R., Li, Z., Kuchta, J., King, G. H., Hayes, A., & Lambert, S. (2013). The spatial and seasonal variation of nitrogen dioxide and sulfur dioxide in Cape Breton Highlands National Park, Canada, and the association with lichen abundance. *Atmospheric Environment, 64*, 303-311. doi:https://doi.org/10.1016/j.atmosenv.2012.09.068

Gilbert, N. L., Goldberg, M. S., Beckerman, B., Brook, J. R., & Jerrett, M. (2005). Assessing Spatial Variability of Ambient Nitrogen Dioxide in Montréal, Canada, with a Land-Use Regression Model. *Journal of the Air & Waste Management Association, 55*(8), 1059-1063. doi:10.1080/10473289.2005.10464708

Goldizen, F. C., Sly, P. D., & Knibbs, L. D. (2016). Respiratory effects of air pollution on children. *Pediatric Pulmonology, 51*(1), 94-108. doi:10.1002/ppul.23262

Gulliver, J., & Briggs, D. J. (2004). Personal exposure to particulate air pollution in transport microenvironments. *Atmospheric Environment, 38*(1), 1-8. doi:10.1016/j.atmosenv.2003.09.036

Hagenbjörk, A., Malmqvist, E., Mattisson, K., Sommar, N. J., & Modig, L. (2017). The spatial variation of O(3), NO, NO(2) and NO (x) and the relation between them in two Swedish cities. *Environmental monitoring and assessment, 189*(4), 161-161. doi:10.1007/s10661-017-5872-z

Hagenbjork-Gustafsson, A., Tornevi, A., Forsberg, B., & Eriksson, K. (2010). Field validation of the Ogawa diffusive sampler for NO2 and NOx in a cold climate. *Journal of Environmental Monitoring, 12*(6), 1315-1324. doi:10.1039/B924615K

Hagenbjork-Gustafsson, A., Tornevi, A., Forsberg, B., & Eriksson, K. (2010). Field validation of the Ogawa diffusive sampler for NO2 and NOx in a cold climate. *J Environ Monit, 12*(6), 1315-1324. doi:10.1039/b924615k

Hargreaves, P. R., Leidi, A., Grubb, H. J., Howe, M. T., & Mugglestone, M. A. (2000). Local and seasonal variations in atmospheric nitrogen dioxide levels at Rothamsted, UK, and relationships with meteorological conditions. *Atmospheric Environment, 34*(6), 843-853. doi:https://doi.org/10.1016/S1352-2310(99)00360-X

Hassan, M., Mumtaz, W., Raza, I., Syed, W. A. A., & Ali, S. S. (2013). APPLICATION OF AIR DISPERSION MODEL FOR THE ESTIMATION OF AIR POLLUTANTS FROM COAL-FIRED BRICK-KILNS SAMPLES IN GUJRAT. *Science International, 25*(1), 141 - 145.

Holman, C. (1999). 8 - Sources of Air Pollution A2 - Holgate, Stephen T. In J. M. Samet, H. S. Koren, & R. L. Maynard (Eds.), *Air Pollution and Health* (pp. 115-148). London: Academic Press.

Huang, L., Zhang, C., & Bi, J. (2017). Development of land use regression models for PM2.5, SO2, NO2 and O3 in Nanjing, China. *Environmental Research, 158*, 542-552. doi:https://doi.org/10.1016/j.envres.2017.07.010

Jerrett, M., Burnett, R. T., Pope, C. A., Ito, K., Thurston, G., Krewski, D., . . . Thun, M. (2009). Long-Term Ozone Exposure and Mortality. *New England Journal of Medicine, 360*(11), 1085-1095. doi:10.1056/NEJMoa0803894

Jerrett, M., Finkelstein, M. M., Brook, J. R., Arain, M. A., Kanaroglou, P., Stieb, D. M., . . . Sears, M. R. (2009). A Cohort Study of Traffic-Related Air Pollution and Mortality in Toronto, Ontario, Canada. *Environmental Health Perspectives, 117*(5), 772-777.

Kanaroglou, P. S., Jerrett, M., Morrison, J., Beckerman, B., Arain, M. A., Gilbert, N. L., & Brook, J. R. (2005). Establishing an air pollution monitoring network for intra-urban population exposure assessment: A location-allocation approach. *Atmospheric Environment, 39*(13), 2399-2409. doi:https://doi.org/10.1016/j.atmosenv.2004.06.049

Kashima, S., Yorifuji, T., Sawada, N., Nakaya, T., & Eboshida, A. (2018). Comparison of land use regression models for NO2 based on routine and campaign monitoring data from an urban area of Japan. *Science of The Total Environment, 631-632*, 1029-1037. doi:https://doi.org/10.1016/j.scitotenv.2018.02.334

Kasparoglu, S., Incecik, S., & Topcu, S. (2018). Spatial and temporal variation of O3, NO and NO2 concentrations at rural and urban sites in Marmara Region of Turkey. *Atmospheric Pollution Research, 9*(6), 1009-1020. doi:https://doi.org/10.1016/j.apr.2018.03.005

Kerckhoffs, J., Wang, M., Meliefste, K., Malmqvist, E., Fischer, P., Janssen, N. A. H., . . . Hoek, G. (2015). A national fine spatial scale land-use regression model for ozone. *Environmental Research, 140*, 440-448. doi:https://doi.org/10.1016/j.envres.2015.04.014

Keuken, M. P., Roemer, M. G. M., Zandveld, P., Verbeek, R. P., & Velders, G. J. M. (2012). Trends in primary NO2 and exhaust PM emissions from road traffic for the period 2000–2020 and implications for air quality and health in the Netherlands. *Atmospheric Environment, 54*, 313-319. doi:https://doi.org/10.1016/j.atmosenv.2012.02.009

Lee, J.-H., Wu, C.-F., Hoek, G., de Hoogh, K., Beelen, R., Brunekreef, B., & Chan, C.-C. (2014). Land use regression models for estimating individual NOx and NO2 exposures in a metropolis with a high density of traffic roads and population. *Science of The Total Environment, 472*, 1163-1171.

Liu, W., Li, X., Chen, Z., Zeng, G., León, T., Liang, J., . . . Lai, M. (2015). Land use regression models coupled with meteorology to model spatial and temporal variability of NO2 and PM10 in Changsha, China. *Atmospheric Environment, 116*, 272-280. doi:https://doi.org/10.1016/j.atmosenv.2015.06.056

Mahajan, A. S., De Smedt, I., Biswas, M. S., Ghude, S., Fadnavis, S., Roy, C., & van Roozendael, M. (2015). Inter-annual variations in satellite observations of nitrogen dioxide and formaldehyde over India. *Atmospheric Environment, 116*, 194-201. doi:https://doi.org/10.1016/j.atmosenv.2015.06.004

Mahata, K. S., Rupakheti, M., Panday, A. K., Bhardwaj, P., Naja, M., Singh, A., . . . Lawrence, M. G. (2018). Observation and analysis of spatiotemporal characteristics of surface ozone and carbon monoxide at multiple sites in the Kathmandu Valley, Nepal. *Atmospheric Chemistry and Physics, 18*(19), 14113-14132. doi:10.5194/acp-18-14113-2018

Maindonald, J. H., & Braun, W. J. (2015). DAAG: Data Analysis and Graphics Data and Functions. Retrieved from https://CRAN.R-project.org/package=DAAG

Malmqvist, E., Olsson, D., Hagenbjörk-Gustafsson, A., Forsberg, B., Mattisson, K., Stroh, E., . . . Modig, L. (2014). Assessing ozone exposure for epidemiological studies in Malmö and Umeå, Sweden. *Atmospheric Environment, 94*, 241-248. doi:https://doi.org/10.1016/j.atmosenv.2014.05.038

Matte, T. D., Ross, Z., Kheirbek, I., Eisl, H., Johnson, S., Gorczynski, J. E., . . . Clougherty, J. E. (2013). Monitoring intraurban spatial patterns of multiple combustion air pollutants in New York City: Design and implementation. *Journal of Exposure Science and Environmental Epidemiology, 23*(3), 223-231. doi:10.1038/jes.2012.126

Meng, X., Chen, L., Cai, J., Zou, B., Wu, C.-F., Fu, Q., . . . Kan, H. (2015). A land use regression model for estimating the NO2 concentration in shanghai, China. *Environmental Research, 137*, 308-315. doi:https://doi.org/10.1016/j.envres.2015.01.003

Miller, K., Siscovick, D., Sheppard, L., Shepherd, K., Sullivan, J., Anderson, G., & Kaufman, J. (2007). Long-term exposure to air pollution and incidence of cardiovascular events in women. *New England Journal of Medicine, 356*(5), 447-458.

Miller, L., Lemke, L. D., Xu, X., Molaroni, S. M., You, H., Wheeler, A. J., . . . Weglicki, L. (2010). Intra-urban correlation and spatial variability of air toxics across an international airshed in Detroit, Michigan (USA) and Windsor, Ontario (Canada). *Atmospheric Environment, 44*(9), 1162-1174. doi:https://doi.org/10.1016/j.atmosenv.2009.12.030

Ministry of Environment. (2011). *State and Trends of the Lebanese Environment*. Retrieved from Beirut, Lebanon:

Moodley, K. G., Singh, S., & Govender, S. (2011). Passive monitoring of nitrogen dioxide in urban air: A case study of Durban metropolis, South Africa. *Journal of Environmental Management, 92*(9), 2145-2150. doi:https://doi.org/10.1016/j.jenvman.2011.03.040

NASA. (2003). Chemistry in the Sunlight. Retrieved from https://earthobservatory.nasa.gov/features/ChemistrySunlight/chemistry_sunlight3.php

Nassar, J. (2016). *Sources, dispersion and toxicity of PAHs and dioxins at AUB, Zouk and Dora.* (Dissertation/Thesis). Retrieved from http://aub.summon.serialssolutions.com/2.0.0/link/0/eLvHCXMwY2AwNtIz0EUrE0zMjJOME5PMgdWLUYqFWWpKoqVlknlKGrB2MQcmC_DdEwGWAZHmEW7GHoizo-EnJpYmgccucpIQYxcWJqZGJsbMDMxGBuB9W6GgU0MSYUd9gqsHN0EGHhekaW0hBqbUPBEGr2DwuHixjkJKJug4btCwlAKw365Qkl-RmQxs_CrkpykEOHoUgwVTMoGieUB2iYJjqJOOQlR-aTZYwgUYR6IMMm6uIc4eukCL46EDLvEwt5kbiTGwADvxqRIMCsZpRmYpKRYpFsD2u4lZUoqlZbKlYZJFKrB_lWiRnGgpySCK1QgpHOIyDKxpwPSZKgv2sxzY_wB3VGjG

Nuvolone, D., Petri, D., & Voller, F. (2018). The effects of ozone on human health. *Environmental Science and Pollution Research, 25*(9), 8074-8088. doi:10.1007/s11356-017-9239-3

Ogawa. (2001). Protocol for Ozone measurement using the ozone passive sampler badge (3 ed.). 665 Huntington Avenue, Boston, MA 02115 USA: Harvard School of Public Health, Environmental Science and Engineering Program, Department of Environmental Health.

OGAWA. (2006). NO, NO2, NOx and SO2 Sampling Protocol Using the Ogawa Sampler (6 ed.).

Parenteau, M., & Sawada, M. C. (2012). The role of spatial representation in the development of a LUR model for Ottawa, Canada. *Air Quality, Atmosphere, & Health, 5*(3), 311 - 323. doi:doi:http://dx.doi.org/10.1007/s11869-010-0094-3

Rahman, M. M., Yeganeh, B., Clifford, S., Knibbs, L. D., & Morawska, L. (2017). Development of a land use regression model for daily NO2 and NOx concentrations in the Brisbane metropolitan area, Australia. *Environmental Modelling & Software, 95*, 168-179. doi:https://doi.org/10.1016/j.envsoft.2017.06.029

RCoreTeam. (2013). R: A Language and Environment for Statistical Computing: R Foundation for Statistical Computing. Retrieved from http://www.R-project.org/

Ripley, B. D., John, W., & Sons. (2004). *Spacial statistics*. Hoboken, NJ: Wiley-Interscience.

Saliba, N. A., Moussa, S., Salame, H., & El-Fadel, M. (2006). Variation of selected air quality indicators over the city of Beirut, Lebanon: Assessment of emission sources. *Atmospheric Environment, 40*(18), 3263-3268. doi:10.1016/j.atmosenv.2006.01.054

Salloum, S., Nassar, J., Baalbaki, R., Shihadeh, A. L., Saliba, N. A., & Lakkis, I. (2018). PM10 Plume dispersion data of the Zouk power plant in Lebanon. *Data in Brief, 20*, 1905-1911. doi:10.1016/j.dib.2018.09.047

Sather, M. E., Slonecker Et Fau - Kronmiller, K. G., Kronmiller Kg Fau - Williams, D. D., Williams Dd Fau - Daughtrey, H., Daughtrey H Fau - Mathew, J., & Mathew, J. Evaluation of short-term Ogawa passive, photolytic, and federal reference method sampling devices for nitrogen oxides in El Paso and Houston, Texas. (1464-0325 (Print)).

Sather, M. E., Slonecker, E. T., Kronmiller, K. G., Williams, D. D., Daughtrey, H., & Mathew, J. (2006). Evaluation of short-term Ogawa passive, photolytic, and federal reference method sampling devices for nitrogen oxides in El Paso and Houston, Texas. *Journal of Environmental Monitoring, 8*(5), 558-563. doi:10.1039/b601113f

Sather, M. E., Slonecker, E. T., Mathew, J., Daughtrey, H., & Williams, D. D. (2007). Evaluation of ogawa passive sampling devices as an alternative measurement method for the nitrogen dioxide annual standard in El Paso, Texas. *Environmental Monitoring and Assessment, 124*(1), 211-221. doi:10.1007/s10661-006-9219-4

Sider, T., Alam, A., Zukari, M., Dugum, H., Goldstein, N., Eluru, N., & Hatzopoulou, M. (2013). Land-use and socio-economics as determinants of traffic emissions and individual exposure to air pollution. *Journal of Transport Geography, 33*, 230-239. doi:10.1016/j.jtrangeo.2013.08.006

Sillman, S. (1999). The relation between ozone, NOx and hydrocarbons in urban and polluted rural environments. *Atmospheric Environment, 33*(12), 1821-1845. doi:https://doi.org/10.1016/S1352-2310(98)00345-8

Stuart, A. L., & Zeager, M. (2011). An inequality study of ambient nitrogen dioxide and traffic levels near elementary schools in the Tampa area. *Journal of Environmental Management, 92*(8), 1923-1930. doi:https://doi.org/10.1016/j.jenvman.2011.03.003

Su, J. G., Jerrett, M., & Beckerman, B. (2009). A distance-decay variable selection strategy for land use regression modeling of ambient air pollution exposures. *Science of The Total Environment*, *407*(12), 3890-3898. doi:10.1016/j.scitotenv.2009.01.061

USEPA. (2018). Managing Air Quality - Control Strategies to Achieve Air Pollution Reduction. Retrieved from https://www.epa.gov/air-quality-management-process/managing-air-quality-control-strategies-achieve-air-pollution#what

Valuntaitė, V., Šerevičienė, V., Girgždienė, R., & Paliulis, D. (2012). *Relative Humidity and Temperature Impact to Ozone and Nitrogen Oxides Removal Rate in the Experimental Chamber* (Vol. 20).

Wang, Y., Yu, C., Tao, J., Wang, Z., Si, Y., Cheng, L., . . . Chen, L. (2018). Spatio-Temporal Characteristics of Tropospheric Ozone and Its Precursors in Guangxi, South China. *Atmosphere*, *9*(9). doi:10.3390/atmos9090355

Weatherbee, S. (2015). Zouk residents decry power plant pollution. *TCA Regional News U6 - ctx_ver=Z39.88-2004&ctx_enc=info%3Aofi%2Fenc%3AUTF-8&rfr_id=info%3Asid%2Fsummon.serialssolutions.com&rft_val_fmt=info%3Aofi%2Ffmt%3Akev%3Amtx%3Ajournal&rft.genre=article&rft.atitle=Zouk+residents+decry+power+plant+pollution&rft.jtitle=TCA+Regional+News&rft.au=Sarah+Weatherbee&rft.date=2015-04-27&rft.pub=Tribune+Content+Agency+LLC&rft.externalDocID=3665855471&paramdict=en-US U7 - Newspaper Article*. Retrieved from http://aub.summon.serialssolutions.com/2.0.0/link/0/eLvHCXMwY2AwNtIz0EUrE0DN4GQjC9PkpGSDFLMUgyRQtZtobpBiaJFibpYCjvgAy4BI8wg3Yw_o4kLQ1hhodMNKSXDRnZKfDBo11zcEtnXNzUHtEfuCQl3QPVKg-VbopRrMDKxGoG3SLAysTq5-AUHwThiw_jXBKHfBlYmbAGTRRzHsmATwKpIk8KBJThLaKY0UOU6QQRBUhBUkFqQWKThCUogQA1NqngiDVlR-abYCsKcNulK0pFghBdh4rFQoAN2YplCQAwxsIDsHkiZFGVTcXEOcPXRhDogHnW6cBqz0iuMR1huLMbDk5eelSjAoWBgZpialmCdbJFokm1gkWSaappolJhsapYAPmbEwkWSQxWuUFAF5aQYuYJibguZajMxlGFhKikpTZYGVfmmSHDQWAPWcokI

Weichenthal, S., Ryswyk, K. V., Goldstein, A., Bagg, S., Shekkarizfard, M., & Hatzopoulou, M. (2016). A land use regression model for ambient ultrafine particles in Montreal, Canada: A comparison of linear regression and a machine learning approach. *Environmental Research*, *146*, 65-72. doi:10.1016/j.envres.2015.12.016

Weissert, L. F., Salmond, J. A., Miskell, G., Alavi-Shoshtari, M., & Williams, D. E. (2018). Development of a microscale land use regression model for predicting NO2 concentrations at a heavy trafficked suburban area in Auckland, NZ. *Science of The Total Environment*, *619-620*, 112-119. doi:https://doi.org/10.1016/j.scitotenv.2017.11.028

WHO. (2005). *WHO Air quality guidelines for particulate matter, ozone, nitrogen dioxide and sulfur dioxide*. Retrieved from

WHO. (2018). Air Pollution. Retrieved from https://www.who.int/airpollution/en/

WHO. (2019). How air pollution is destroying our health. Retrieved from **https://www.who.int/air-pollution/news-and-events/how-air-pollution-is-destroying-our-health**

Wolf, K., Cyrys, J., Harciníková, T., Gu, J., Kusch, T., Hampel, R., . . . Peters, A. (2017). Land use regression modeling of ultrafine particles, ozone, nitrogen oxides and markers of particulate matter pollution in Augsburg, Germany. *Science of The Total Environment, 579*, 1531-1540. doi:https://doi.org/10.1016/j.scitotenv.2016.11.160

Xie, X., Semanjski, I., Gautama, S., Tsiligianni, E., Deligiannis, N., Rajan, R. T., . . . Philips, W. (2017). A review of urban air pollution monitoring and exposure assessment methods. *ISPRS International Journal of Geo-Information, 6*(12), 389. doi:10.3390/ijgi6120389

Yang, Y., Liu, X., Zheng, J., Tan, Q., Feng, M., Qu, Y., . . . Cheng, N. (2018). Characteristics of one-year observation of VOCs, NOx, and O3 at an urban site in Wuhan, China. *Journal of Environmental Sciences*. doi:https://doi.org/10.1016/j.jes.2018.12.002

Zeng, X. T., Tong, Y. F., Cui, L., Kong, X. M., Sheng, Y. N., Chen, L., & Li, Y. P. (2017). Population-production-pollution nexus based air pollution management model for alleviating the atmospheric crisis in Beijing, China. *Journal of Environmental Management, 197*, 507-521. doi:https://doi.org/10.1016/j.jenvman.2017.04.022

Zhao, T., Markevych, I., Romanos, M., Nowak, D., & Heinrich, J. (2018). Ambient ozone exposure and mental health: A systematic review of epidemiological studies. *Environmental Research, 165*, 459-472. doi:https://doi.org/10.1016/j.envres.2018.04.015

Zhu, Y., Zhan, Y., Wang, B., Li, Z., Qin, Y., & Zhang, K. (2019). Spatiotemporally mapping of the relationship between NO2 pollution and urbanization for a megacity in Southwest China during 2005–2016. *Chemosphere, 220*, 155-162. doi:https://doi.org/10.1016/j.chemosphere.2018.12.095